Photoswitchable assembly of long-lived azobenzenes in water using visible light

Camille Courtine, Inès Hamouda, Samuel Pearson, Laurent Billon, Pierre Lavedan, Sonia Mallet-Ladeira, Jean-Claude Micheau, Véronique Pimienta, Erwan Nicol, Nancy Lauth de Viguerie, et al.

Photoswitchable assembly of long-lived azobenzenes in water using visible light

Camille Courtine[a], Inès Hamouda[b], Samuel Pearson[c,d, ‡], Laurent Billon[c,d], Pierre Lavedan[e], Sonia Ladeira[f], Jean-Claude Micheau[a], Véronique Pimienta[a], Erwan Nicol[b], Nancy Lauth de Viguerie[a, *] and Anne-Françoise Mingotaud[a, *]

a. Laboratoire des IMRCP, Université de Toulouse, CNRS UMR 5623, Université Toulouse III - Paul Sabatier, 118 Rte de Narbonne, 31062 Toulouse cedex 9, France.

b. Institut des Molécules et Matériaux du Mans (IMMM), UMR CNRS 6283, Equipe Polymères, Colloïdes, Interfaces, Le Mans Université, Avenue Olivier Messiaën 72085 Le Mans Cedex 9, France

c. Université de Pau & Pays Adour, CNRS, IPREM UMR 5254, 2 Avenue du Président Angot, Pau F-64053, France

d. Bio-inspired Materials Group, Functionality & Self-assembly, Université de Pau & Pays Adour, 2 Avenue du President Angot, Pau F-64053, France

e. Paul Sabatier University - Toulouse III | UPS Toulouse · Institut de Chimie de Toulouse ICT - FR 2599

f. Institut de Chimie de Toulouse (UAR, 2599), 118, Route de Narbonne, 31062 Toulouse Cedex 09, France

‡ present address: INM – Leibniz Institute for New Materials, Campus D2 2, 66123, Saarbrücken, Germany

E-mail addresses : camillec.mail@gmail.com, Ines.Hamouda@univ-lemans.fr, Samuel.Pearson@leibniz-inm.de, laurent.billon@univ-pau.fr, lavedan@chimie.ups-tlse.fr, sonia.ladeira@univ-tlse3.fr, jean-claude.micheau@univ-tlse3.fr, veronique.pimienta@univ-tlse3.fr, erwan.nicol@univ-lemans.fr, nancy.de-viguerie@univ-tlse3.fr, anne-francoise.mingotaud@cnrs.fr

Corresponding authors: Nancy Lauth de Viguerie and Anne-Françoise Mingotaud

Tel: (33) 561 55 61 35 or (33) 561 55 62 72

Abstract

Hypothesis: Switchable assemblies relevant for bio-applications may be accessed from water-soluble tetra-*ortho*-substituted azobenzenes that reversibly self-assemble and form complexes with β-cyclodextrin under visible light.

Experiments: Two azobenzenes bearing either four fluorines or two chlorines and two fluorines in the *ortho* positions were synthesised with short poly(ethylene oxide) tails for water solubility. Photophysical properties were determined by UV-Vis and ^{1}H NMR spectroscopies, complexation with β-cyclodextrin was assessed by ^{1}H NMR spectroscopy, and self-assembly in water was investigated by static and dynamic light scattering.

Findings: Both molecules underwent *trans-cis* isomerization at 530 nm and *cis-trans* isomerization at 415 nm, with the *cis* forms exhibiting thermal half-lives > 300 days at room temperature. Both molecules formed inclusion complexes with β-cyclodextrin in water, with *cis*-4F-AZO-PEO binding 3-fold stronger than *trans*, and 2Cl2F-AZO-PEO binding significantly weaker. Self-assembly of pure 2Cl2F-AZO-PEO in water showed an open association process regardless of configuration, while 4F-AZO-PEO showed an open association process for *cis* (N_{agg} increasing from 30 to 1000) but a closed association process for *trans* (N_{agg} stable at ~ 170). Aqueous solutions of 2Cl2F-AZO-PEO showed cloud points close to 45°C, while the 4F-AZO-PEO isomers presented well-separated cloud points allowing reversible and all-visible transition between clear and turbid states at room temperature.

Graphical abstract
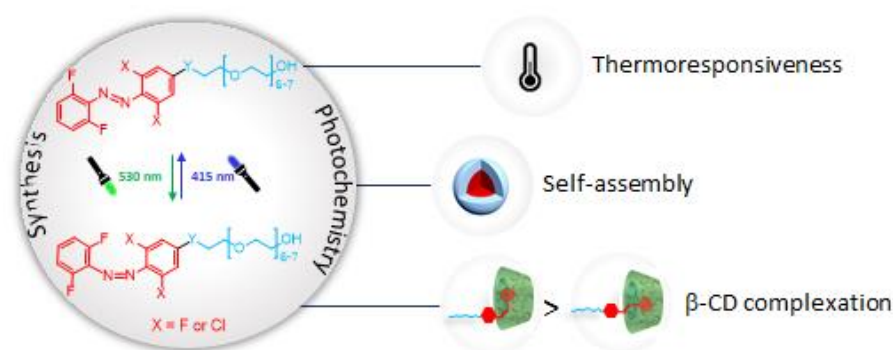
Keywords: azobenzene, photoswitch, photoresponsive, cyclodextrin, photochemistry, self-assembly, cloud point.

I.   Introduction

The field of active soft matter has given rise to many exciting functional devices and materials, such as artificial muscles, autonomous swimmers and photo-tunable self-assemblies.[1-3] Azobenzenes are reversible photochemical switches that undergo light-driven *trans–cis* isomerization and are often employed in such systems. Their synthetic accessibility, fast and reversible photoswitching, and low rate of photobleaching have made azobenzenes appealing components of countless molecular devices[4] and photo-responsive materials.[5] Isomerization is accompanied by a change in polarity and geometry, which can both be exploited on different length scales, from molecular switches for photopharmacology, to dissociable polymeric drug delivery systems, or macroscopic light-harvesting materials.[6-11] Beyond their photochemical properties, azobenzenes are also able to form association complexes with different hosts, such as cyclodextrins (CD)[12, 13] or cucurbituril.[14, 15] For β-CD in particular, *trans* isomers of traditional azobenzenes can access and interact strongly with the hydrophobic cavity (Ka ~ 2.5 x 10^3 M^{-1})[16] while *cis* forms are unable to enter (Ka too small to measure).[17] The disparate binding abilities of the two isomers with β-CD has been exploited in numerous photoresponsive (bio)materials, such as hydrogels capable of reversible stiffness modulation[18] or drug release,[19] antimicrobial[20] and cell capture/release surfaces,[21] and detachable/replaceable nanomotors.[22]

Despite their advantages, unsubstituted azobenzenes typically require UV light to drive *trans-cis* isomerization (via π→π* excitation). Moreover, the reverse *cis-trans* isomerization using blue light (via n→π* excitation) is typically far from complete due to overlapping of the n→π* absorption bands of each isomer. For biological applications, the toxicity and poor penetration depth of UV light is particularly restrictive,[23] limiting the application of traditional azobenzenes *in vivo*. Water solubility is also usually limited,[24, 25] and is obtained by the introduction of polar groups such as carboxylate[26] or ether groups.[27]

In pursuit of more biologically applicable azobenzenes, the last decade or so has seen major breakthroughs in the development of azobenzenes that can be switched in both directions at visible wavelengths.[28] In particular, tetra-*ortho*-substituted azobenzenes bearing electron-donating/σ-electron-withdrawing substituents such as methoxy,[29] thioether,[30] hydropropoxy,[31] fluoro,[32] chloro,[33] or bromo groups in the *ortho* positions exhibit red-shifted n→π* bands in the *trans* isomer. This n→π* band is then separated from that of the *cis* isomer and allows *trans-cis* isomerization using long wavelengths up to near-infrared (NIR) in some cases. While the older strategy of red-shifting the π→π* transition into the visible by introducing push-pull substituents drastically shortens the *cis* isomer half-life,[34] the new generation of tetra-*ortho*-substituted azobenzenes (and derivatives) exhibit remarkably stable *cis* isomers.

The excitement over red-shifted tetra-*ortho*-substituted azobenzenes arises from new possibilities now available in the biological domain, with systems such as controlled bioadhesive surfaces[35] and photoswitchable therapeutic molecules[36] benefitting from long-wavelength visible activation, almost complete photoswitching, and high thermal stability of the *cis* isomer that were previously unattainable. Applications beyond the biological realm can also benefit from visible photoswitching, such as energy harvesting.[37] Low yields of these

azobenzenes in some of the pioneering reports[29, 32] have been addressed with improved synthesis protocols,[38] and the resulting myriad of derivatives bearing different substitution patterns have been systematically explored to better understand the electronic contributions that underpin their photophysical performance.[30, 34, 39] Although tetra-*ortho*-fluoro azobenzenes have been most widely adopted, two recent papers have explored "mixed" dichloro difluoro azobenzenes possessing one halogen type on each aromatic ring.[40, 41] With this configuration of *ortho*-halogen atoms, high separation of the n→π* bands of *cis* and *trans*, photoswitching with deep red wavelengths, and an extremely stable *cis* form were achieved. In the present work, we explore a dichloro difluoro azobenzene in which each aromatic ring has the same halogen type in *ortho* positions. Feringa and coll. presented such a 2Cl2F-substituted azobenzene, but no photophysical studies were performed.[38]

In previous work, we developed UV-responsive hydrogels exploiting azobenzene-CD complexes and explored thermodynamics and kinetics of complexation.[18, 27] In this work we aimed to develop all-visible associative azobenzene systems using tetra-*ortho*-substituted species. We compare a tetra-*ortho*-fluoro azobenzene derivative that has some close relatives in literature with a less-explored 2Cl2F-AZO derivative, both bearing poly(ethylene oxide) (PEO) tails to impart water solubility. We present a straightforward synthesis sequence for obtaining the 2Cl2F photoswitch with functionalizable carboxylic acid handle in the *para*-position to which we attached the PEO chain. The photophysical and associative properties of these two azobenzenes in water are explored, in particular their complexation with β-CD and their self-assembly behaviour including the formation of photoswitchable aggregates.

2. Materials and Methods

2.1. Reagents

Deuterium solvents were purchased from Eurisotop. β-cyclodextrin (98% purity, with 11.7 % $_{wt}$ of water, determined by Karl Fisher titration) was purchased from Fluka (Germany). All solvents and reagents (ACS grade) were used as received unless otherwise specified.

2.2. Syntheses

2.2.1. Ethyl 3,5-dichloro-4-aminobenzoate (**1**)

Adapted from Bléger et al.[32] 2,6-Dichloro-4-carboxyaniline (15.0 g, 72.8 mmol, 1.0 equiv.) was dissolved in EtOH (300 mL) and conc. H_2SO_4 (5.8 mL, 109.2 mmol, 1.5 equiv.) was added. The solution was refluxed for 12 h, by which point thin layer chromatography (TLC) (dichloromethane (DCM)/MeOH 95:5 $_{v/v}$) showed full consumption of the starting material (R_f = 0.05) and formation of a single new product (R_f = 0.95). The solution was neutralized with saturated $NaHCO_3$, extracted with DCM, and the organic phase was dried with $MgSO_4$. The solid was filtered off, and the solvent was removed by rotary evaporator to give the desired product **1** as a pale-yellow solid (17.0 g, 100 %).

^{1}H NMR (400 MHz, CDCl$_3$) δ (ppm): 7.88 (s, 2H, Ar-H), 4.87 (br s, 2H, NH$_2$), 4.33 (q, 2H, J = 7.2 Hz, -CH_2CH$_3$), 1.37 (t, 3H, J = 7.2 Hz, CH$_2$CH_3).

2.2.2. Ethyl 3,5-dichloro-4-nitrosobenzoate (2)

Adapted from Holmes and Bayer.[42] To compound **1** (8.0 g, 34.2 mmol, 1.0 equiv.) was added acetic acid (67.3 mL, 598 mmol, 17.5 equiv.), 30 % $_{v/v}$ H$_2$O$_2$ (16.7 mL, 147 mmol, 4.3 equiv.), and conc. H$_2$SO$_4$ (1.0 mL, 19 mmol, 0.6 equiv.). A septum was fitted and the suspension was degassed for 10 min using nitrogen bubbling, then warmed gently with magnetic stirring in an oilbath at 60 ° C until the solid dissolved. Once dissolved, the solution was removed from the oilbath and stirred at room temperature (r.t.) for 3 days, during which a colourless crystalline solid gradually precipitated from the pale green solution. The solid was isolated by filtration, washed with minimum cold MeOH, and dried under vacuum. The solid was redissolved in DCM (100 mL), washed with saturated bicarbonate solution (2 x 100 mL) then brine (100 mL), and the green organic phase was separated and dried with MgSO$_4$. The solid was filtered off, and the solvent was removed under vacuum to give the desired product **2** in its more stable dimeric form [42] as colourless crystals (6.91 g, 82 %). Note: TLC (cyclohexane/DCM 1:1 v/v) showed some starting material (R$_f$ = 0.6) remaining in the reaction solution after 3 days, and small-scale reactions performed for longer reaction times (7 days) reached higher yields (> 85 %).

^{1}H NMR (400 MHz, CDCl$_3$) δ (ppm): 8.14 (s, 1.67H, Ar-H), 4.44 (q, 2H, J = 7.2 Hz, -CH_2CH$_3$), 1.44 (t, 3H, J = 7.2 Hz, -CH$_2$CH_3). Note: The aromatic signal corresponds to the dimeric species that typically predominates in nitrosoarenes,[42] here 84 %, with a separate aromatic peak at 8.10 ppm (s, 0.33H, Ar-H) corresponding to the undimerized nitrosoarene (16 %). Chemical shifts of the remaining protons are indistinguishable between the two species.

^{13}C NMR (100 MHz, CDCl$_3$) δ (ppm): 163.18, 140.58, 134.58, 131.52, 130.39, 62.64, 14.33. Note: The reported peaks are for the predominant dimer, with two minor peaks attributed to the undimerized species at δ (ppm): 163.25, 134.94. The remaining peaks are common to both species. See Figure S1 for spectra.

2.2.3. Ethyl 4-[(1E)-2-(2,6-difluorophenyl)diazenyl]-3,5-dichlorobenzoate (3)

Adapted from Knie *et al.*[39] To compound **2** (6.91 g, 27.8 mmol, 1.0 equiv.) was added acetic acid (128.5 mL), toluene (128.5 mL), and trifluoroacetic acid (21.4 mL). A septum was fitted, and the suspension was degassed for 10 min using nitrogen bubbling, then placed in an oilbath at 60 °C with magnetic stirring until the solid dissolved. Once the solid had dissolved, 2,6-difluoroaniline (3.60 mL, 33.4 mmol, 1.2 equiv.) was added, and the solution was stirred for 3 days at 60 °C, during which it changed colour from dark green to orange/black. Throughout the reaction aliquots were periodically taken, dried under vacuum, and analyzed by ^{1}H NMR spectroscopy (CDCl$_3$) to monitor the reaction progress until **2** was essentially consumed. The solution was poured into water (200 mL), and extracted with Et$_2$O (100 mL). The organic phase was washed with saturated sodium bicarbonate solution (3 x 100 mL), brine (100 mL), and then

dried with MgSO₄ and filtered. The solvent was removed under vacuum. The crude solid was redissolved in acetone (50 mL) and adsorbed on silica for column chromatography using toluene as eluant (R_f = 0.7), which gave better separation from the slower-moving byproducts than more common eluant choices. The combined product fractions were evaporated to dryness to give the desired product **3** as a reddish-brown solid (4.80 g, 48 %). Care should be taken in the steps up until the silica column to minimize ambient light exposure, which can generate the slower-moving *cis* isomer and hinder the purification.

¹H NMR *E*-isomer (400 MHz, CDCl₃) δ (ppm): 8.10 (s, 2H, Ar-H), 7.48 – 7.43 (m, 1H, Cl-Ar-H), 7.14 – 7.09 (apparent t, 2H, *J* = 8.9 Hz, F-Ar-H), 4.45 – 4.39 (q, 2H, *J* = 7.2 Hz, -C*H₂*CH₃), 1.45 – 1.41 (t, 3H, *J* = 7.2 Hz, -CH₂C*H₃*). *Z*-isomer δ (ppm): 7.92 (s, 2H, Ar-H), 7.28 – 7.18 (m, 1H, Cl-Ar-H), 6.87 – 6.83 (qt, 2H, F-Ar-H), 4.39 – 4.34 (q, 2H, *J* = 7.2 Hz, -C*H₂*CH₃), 1.41 – 1.37 (t, 3H, *J* = 7.2 Hz, -CH₂C*H₃*).

¹³C NMR *E*-isomer (100 MHz, CDCl₃) δ (ppm): 164.06, 157.38, 154.76, 151.82, 132.86 (t, $J_{C\text{-}F}$ = 10.5 Hz), 131.29, 130.32, 126.75, 112.97 (dd, $J_{C\text{-}F}$ = 20.9 Hz, $J_{C\text{-}F}$ = 3.8 Hz), 62.13, 14.39. Note: Some peaks distinct to the *Z*-isomer are also observed at δ (ppm): 131.03 (apparent t, $J_{C\text{-}F}$ = 10.5 Hz), 129.99, 112.43 (dd, *J* = 20.9 Hz, *J* = 3.8 Hz). See Figure S2 for spectra.

2.2.4. 4-[(1*E*)-2-(2,6-difluorophenyl)diazenyl]-3,5-dichloro-benzoic acid (**4**)

Compound **3** (4.58 g, 12.6 mmol, 1.0 equiv.) was dissolved in THF (40 mL) and a solution of KOH (2.50 g, 44.6 mg, 3.5 equiv.) dissolved in water (80 mL) was added. The mixture was stirred in an oilbath at 70 °C, at which point TLC (toluene) showed no fast-moving starting material (R_f = 0.7) and all red colour remaining on the baseline. The reaction mixture was allowed to cool, and was transferred to a separating funnel containing water (100 mL) and EtOAc (200 mL). The aqueous phase was neutralised by adding 1 M HCl before extracting the product into the organic phase. The aqueous phase was washed once more with EtOAc (50 mL), and the combined organic portions were washed with brine (100 mL), dried with MgSO₄, and filtered. The solvent was removed under vacuum to give the product **4** as a reddish-brown solid (4.14 g, 98 %).

¹H NMR *E*-isomer (400 MHz, d₆-DMSO) δ (ppm): 8.10 (s, 2H, Ar-H), 7.76 – 7.70 (m, 1H, Cl-Ar-H), 7.45 – 7.41 (apparent t, 2H, F-Ar-H).

¹³C NMR (100 MHz, CDCl₃) δ (ppm): 164.56, 156.24, 153.65, 150.49, 134.72 (t, $J_{C\text{-}F}$ = 10.5 Hz), 132.57, 130.05, 125.41, 113.47 (dd, *J* = 20.9 Hz, *J* = 3.8 Hz). See Figure S3 for spectra.

2.2.5. 4-[(1*E*)-2-(2,6-difluorophenyl)diazenyl]-*N*-(23-hydroxy-3,6,9,12,15,18,21-heptaoxatricos-1-yl)-3,5-dichlorobenzamide (2Cl2F-AZO-PEO)

23-Amino-3,6,9,12,15,18,21-heptaoxatricosan-1-ol (H₂N-PEO₈-OH, 0.547 g, 1.48 mmol, 1.00 equiv.) was dissolved in dry DCM (10 mL) under N₂, and the solution was added to a N₂-purged flask fitted with magnetic stir bar containing compound **4** (0.50 g, 1.51 mmol, 1.02 equiv.). The solution was cooled in a salt/ice bath for 5 min, then a solution of dicyclohexyl carbodiimide (DCC) (0.312 g, 1.51 mmol, 1.02 equiv.) in dry DCM (4 mL) was added dropwise. After complete addition of the DCC solution, the reaction mixture was allowed to warm to room

temperature and stirred overnight. The next day, the white dicyclohexylurea byproduct was filtered off, and the supernatant was adsorbed on silica under reduced pressure. Silica gel column chromatography using a gradient eluant (DCM/MeOH 96:4 to 94:6 $_{v/v}$) and removal of solvent under reduced pressure gave the pure product (R_f = 0.45 in DCM/MeOH 91:9 $_{v/v}$) as a red oil (0.781 g, 77 %).

^{1}H NMR *E*-isomer (300 MHz, CD$_2$Cl$_2$) δ (ppm): 7.96 (s, 2H, Cl-Ar-H), 7.56 – 7.46 (m, 1H, F Ar-H), 7.40 – 7.30 (br t, 1H, NH), 7.17 – 7.11 (apparent t, 2H, F Ar-H), 3.65 – 3.55 (m, 32H, 16 x -CH$_2$-), 2.68 (br s, 1H, OH. Note: The *Z*-isomer has distinct peaks at δ (ppm): 7.79 (s, 2H, Cl-Ar-H), 7.40 – 7.30 (br t, 1H, NH), 7.35 – 7.24 (m, 1H, F-Ar-H), 6.91 – 6.85 (apparent t, 2H, F-Ar-H).

^{13}C NMR *E*-isomer (75 MHz, CD$_2$Cl$_2$) δ (ppm): 164.41, 157.95, 154.54, 150.64, 136.16 (no H), 133.26 (t, $J_{C\text{-}F}$ = 10.5 Hz), 128.61, 126.93, 113.22 (dd, $J_{C\text{-}F}$ = 20.2 Hz, $J_{C\text{-}F}$ = 3.5 Hz), 72.91, 70.86, 70.67, 69.90, 62.00, 40.67. Note: The *Z*-isomer has distinct peaks at δ (ppm): 128.29, 125.17, 112.72 (dd, $J_{C\text{-}F}$ = 20.9 Hz, $J_{C\text{-}F}$ = 3.8 Hz). See Figure S4 for spectra.

2.3. Characterizations

2.3.1 X-Ray diffraction

Crystals of *trans*-**4** were prepared from ethylacetate solution and X-ray diffraction (XRD) was performed at 193(2) K with a Bruker-AXS D8-Venture using MoK$_\alpha$ radiation (λ=0.71073 Å) and equipped with a PHOTON III detector. Phi- and omega-scans were used. Empirical absorption correction was employed (Bruker, *SADABS*, Bruker AXS Inc., Madison, Wisconsin, USA, 2008). The structure was solved using an intrinsic phasing method (SHELXT),[43] and refined using the least-squares method on F^2.[44] All non-H atoms were refined with anisotropic displacement parameters. All hydrogen atoms bonded to carbon atoms were refined isotropically at calculated positions using a riding model. The hydrogen atom of the hydroxyl group was located in difference-Fourier maps and refined with an isotropic displacement parameter U_{iso}(H) = 1.5U_{eq}(O).

Crystallographic details for **4**: C$_{13}$H$_6$Cl$_2$F$_2$N$_2$O$_2$, M = 331.10, a = 6.7893(16) Å, b = 12.978(3) Å, c =14.828(3) Å, $\alpha = \gamma$ = 90°, β = 95.796(7) °, V = 1299.8(5) Å^3, Z = 4, crystal size 0.20 x 0.10 x 0.08 mm^3, 30859 reflections collected (3095 independent, R$_{int}$ = 0.0257), 193 parameters, R1 [I>2σ(I)] = 0.0274, wR2 [all data] = 0.0724, largest diff. peak and hole: 0.302 and -0.289 eÅ^{-3}.

CCDC 2175884 contains the supplementary crystallographic data for this paper. These data can be obtained free of charge from The Cambridge Crystallographic Data Centre via www.ccdc.cam.ac.uk/data_request/cif.

2.3.2. Photostationary state

The photoisomerization of tetra-*ortho*-fluoro azobenzene poly(ethylene oxide) (4F-AZO-PEO) and di-*ortho*-chloro di-*ortho*-fluoro azobenzene poly(ethylene oxide) (2Cl2F-AZO-PEO) was

followed by UV/Vis spectroscopy (HP 8452A Diode-Array spectrophotometer, Hewlett-Packard, USA) and the photostationary state (PSS) were quantified by ^{1}H NMR spectroscopy (Bruker AVANCE, 500 MHz equipped with a 5 mm Z-gradient TCI cryoprobe and with a 5 mm Z-gradient PRODIGY cryoprobe). The samples were prepared at 0.10 mM in 1 mL of D_2O. Irradiation was performed with a WheeLED^{TM} system from Mightex$^®$ equipped with 530 nm (WLS-LED-0530-03, Mightex, 30 mW•cm^{-2}) and 415 nm (WLS-LED-0415-03, Mightex, 90 mW•cm^{-2}) LEDs to attain the *cis*-rich and *trans*-rich PSS respectively. The evolution of the absorbance of the samples was monitored over the irradiation time by UV/Vis spectroscopy, and once no further change was observed with irradiation time, the percentage of each isomer in the mixture was determined by ^{1}H NMR spectroscopy by integrating the aromatic protons distinct to each isomer between 6.5 and 7.5 ppm. Absorption spectra of the pure isomers were extrapolated from the UV/Vis spectra of the *cis* and *trans* isomers based on their PSS compositions found by NMR spectroscopy.

2.3.3. Thermal stability of *cis* isomers

For compound **3**, ca. 10 mg was dissolved in CD_3CN (0.6 mL) was prepared in an NMR tube. A *cis*-rich mixture was then obtained, *e.g.* by irradiating with a 590 nm LED (~3 mW•cm^{-2}) for 2 h. The tube was then placed in the NMR instrument (Bruker AVANCE 400 MHz) with the sample chamber set to the desired temperature, and a series of consecutive ^{1}H NMR spectra was recorded.

For 4F-AZO-PEO and 2Cl2F-AZO-PEO, the thermal stability of the *cis* isomers was assessed by irradiating aqueous solutions (0.1 mM) for 5 min at 365 nm (for 4F-AZO-PEO) and 530 nm (for 2Cl2F-AZO-PEO) to attain *cis*-rich PSS compositions. The samples were then heated at four different temperatures (37 °C, 60 °C, 70 °C and 80 °C) in the dark and the thermal *cis-trans* isomerization was monitored over time by measuring the absorbance at 350 nm by UV/Vis spectroscopy using a HP 8452A Diode-Array spectrometer. For the experiment at 60 °C, the solutions were heated *in situ* using a Cary 100 Bio UV-Visible spectrometer (Varian, USA) equipped with a temperature controller and a magnetic stirrer and the absorbance was recorded at 300 and 350 nm under stirring. The absorbance was plotted as a function of time for each temperature and the curve fitted with a first order exponential decay function using Origin software to give the rate constant (k) of the thermal isomerization using Equation 1:

$$y = A•e^{-kt}$$ (1)

Half-life ($t_{1/2}$) was then deduced from $t_{1/2} = \ln2/k$

2.3.4. Stoichiometry of AZO@β-cyclodextrin host-guest complexes

The stoichiometry of the complexes formed by 4F-AZO-PEO and 2Cl2F-AZO-PEO with β-cyclodextrin (β-CD) was studied by the Job plot method using ^{1}H NMR spectroscopy (Bruker AVANCE, 500 MHz). *Trans*-rich stock solutions of 4F-AZO-PEO (91% *trans*), 2Cl2F-AZO-PEO (83% *trans*) and β-CD were prepared in D_2O, all at a concentration of 0.30 mM. *Cis*-rich solutions of 4F-AZO-PEO (86% *cis*) and 2Cl2F-AZO-PEO (67% *cis*) were obtained by irradiating *trans*-rich solutions as mentioned in Section 2.3.3. For each analysis solution, an

aliquot of β-CD solution was added to an aliquot of the AZO solution to give the desired AZO:β-CD molar ratio (10:0, 9:1, 8:2, 7:3, 6:4, 5:5, 4:6, 3:7, 2:8, 1:9 and 0:10). Since the intensity of the aromatic signals at the working concentration are very low compared to the intensity of the residual signal of D_2O, this one needed to be removed from the spectrum. The residual signal of D_2O was eliminated by first recording a ^1H NMR spectrum (without D_2O suppression) to identify the exact chemical shift of D_2O in each sample, then obtaining a subsequent spectrum suppressing this signal. Job plots were given by plotting X_{AZO} x $\Delta\delta$ as function of $X_{\beta-CD}$, where X_{AZO} and $X_{\beta-CD}$ are the mole fraction of AZO and of β-CD respectively, and $\Delta\delta$ is the shift observed between the signal of the pure AZO in solution (6.5-7.5 ppm) and after the addition of β-CD.

2.3.5. Association constants of AZO@β-CD complexes determined by numerical modeling

The association constants of the 4F-AZO-PEO@β-CD and 2Cl2F-AZO-PEO@β-CD complexes were determined by UV-visible spectroscopy. The AZOs were dissolved in distilled water at 0.1 mM, and were titrated with β-CD (4F-AZO-PEO:β-CD = 1:0, 1:0.5, 1:1, 1:2, 1:5, 1:10, 1:20, 1:40, 1:50, 1:80 and 1:100; 2Cl2F-AZO-PEO:β-CD = 1:0, 1:1, 1:2, 1:10, 1:40, 1:80 and 1:100). The UV-visible spectra of the samples were recorded using a HP 8452A Diode-Array spectrometer. For each complex, the wavelength at which the spectra of the free AZO and the complex showed the greatest difference was chosen to plot the evolution of the absorbance with β-CD addition. The association constants (Ka) were calculated by modeling this plot following the method described by Thordarson,[45] using a homemade software SA[27] (details are available in SI). This program was employed to fit the equilibrium. The corresponding kinetic equations were integrated for each point until the equilibrium was reached. The differential equations were integrated numerically using a semi-implicit Runge − Kutta method. For a set of given parameters, the calculated values for equilibrium were compared to the experimental data points. The fitted parameters were obtained with a Powel type iterative algorithm designed to minimize the root mean square deviation (Equation 2):

$$\text{RMSD} = \sum_i \sum_j \frac{(c_{ij}e_{ij})^2}{(n.N)} \tag{2}$$

Where c_{ij} and e_{ij} are the calculated concentration and the experimental concentration respectively, n is the number of experimental points and N the number of trials.

2.3.6. Surface tension analysis

Cis-rich and *trans*-rich PSSs were obtained by irradiating the solutions 15 min at 530 nm and 415 nm respectively. Surface tension measurements of *trans*-rich and *cis*-rich 4F-AZO-PEO and 2Cl2F-AZO-PEO from 0.01 to 5 mmol.L^{-1} in water were performed using a pendant drop tensiometer Sinterface PAT1M. The air-water surface tension of 2Cl2F-AZO-PEO solutions was measured by tensiometry at 23 °C for a drop volume of 12 µL. Surface tension values were

recorded for 5 minutes. The final value was calculated as the average of the measurements taken between 3 and 5 minutes. The 4F-AZO-PEO solutions were analyzed at 4 °C for a drop volume of 10 µL. Surface tension values were recorded for around 30 sec, until the drop became cloudy. The final value was calculated as the average of the measurements taken between 10 and 20 seconds.

2.3.7. Cloud point determination

The temperature dependence of 4F-AZO-PEO and 2F-2Cl-AZO-PEO solubility in water was determined by turbidity measurements using a UV-Vis spectrophotometer (Jasco V-760). Solutions with concentrations ranging from 1 to 10 mM were prepared in water from a filtered (0.2 µm inorganic membrane filter) stock solution. To achieve a *cis*-rich PSS, each solution was irradiated using a Thorlabs DC2200 generator at 530 nm (Thorlabs M530L4, 35 mW•cm^{-2}) with stirring at room temperature for 15 min (Figure S5). Each sample was then directly placed in the UV/Vis spectrophotometer sample holder pre-set to 5 °C, and the transmittance was measured at λ=700 nm under stirring as the sample was heated from 5 to 60°C at 0.5 °C/min. The cloud point was given by the transition from limpid to turbid. For each solution, a *trans*-rich PSS was generated by irradiating at 415 nm (Thorlabs M415LP1, 65 mW•cm^{-2}), and the transmittance as a function of temperature was determined in an identical manner to above.

2.3.8. Static and dynamic light scattering analysis

Apparent molar masses (M_{app}) and hydrodynamic radii (R_h) of the molecules in water were assessed by static (SLS) and dynamic (DLS) light scattering. Data were recorded with an ALV-5000 multibit (ALV-GmbH, Germany), multitau, full digital correlator in combination with a Spectra-Physics laser (emitting vertically polarized light at λ= 632.8 nm) and a thermostat bath controlled from 10 to 40 ± 0.2 °C. The measurements were made at detection angles (θ) ranging between 20 ° and 150 °. The sample concentration varied between 2 and 18 mM. Before measurement, all the samples were filtered using 0.2 µm inorganic membrane filter. Complexes of 4F-AZO-PEO with β-CD at a ratio of 1:1 were also analyzed by SLS and DLS. Briefly, a 0.2 µm filtered β-CD solution at 11.40 g.L^{-1} was added to a 0.2 µm filtered PSS(415)$_{trans}$ 4F-AZO-PEO at 10 mM. This mixture was then filtered again on 0.2 µm inorganic membrane filter before measurement at 10 °C. The average relaxation rate (Γ) was found to be linearly proportional to q^2 (where q is the scattering vector).

The cooperative diffusion coefficient (D_c) was calculated as: $D_c = \Gamma/q^2$. At sufficiently low concentrations, where interactions are negligible, the z-average apparent hydrodynamic radius (R_h) of the solute can be calculated from the diffusion coefficient (D_c) using the Stokes-Einstein relation[46].

The normalized excess scattered light, R in cm^{-1}, scattered by the polymer was determined according to Equation 3.

$$R = \frac{R_{solution}(\theta) - R_{solvent}(\theta)}{R_{toluene}(\theta)} \times \left(\frac{n_{Solvent}}{n_{toluene}}\right)^2 \times R_{toluene} \qquad (3)$$

With $R_{solution}$, $R_{solvent}$ and $R_{toluene}$ the average intensities scattered, respectively, by the solution, the solvent, and the reference (toluene) at angle θ; $n_{solvent} = 1.33$ for water and $n_{toluene} = 1.496$ correspond to the respective refractive indexes of water and toluene; and $R_{toluene} = 1.35 \times 10^{-5}$ cm^{-1} the Rayleigh ratio of toluene for a wavelength $\lambda = 632.8$ nm. The normalized excess scattered light R obtained from SLS experiments is related to the polymer concentration (C) in g•cm^{-3}, to a contrast factor K, to the apparent weight average molecular weight of the scatterers extrapolated to q $\rightarrow$ 0 (*i.e*, M_{app}), and to their form factor P(q). Note that M_{app} corresponds to the true molecular weight (M_w) only in very dilute solutions where the interactions between the scatterers can be neglected (Equations 4 and 5):

$$R = K \cdot C \cdot M_{app} \cdot P(q) \qquad (4)$$

$$K = \frac{4\pi^2 n_{solvent}^2}{\lambda^4 N_a} \times \left(\frac{dn}{dC}\right)^2 \qquad (5)$$

Where N_a is Avogadro's number and *dn/dc* the refractive index increment of the polymer in the solvent.

The inverse of the normalized excess scattered light is related to the M_w and to the radius of gyration (R_g) according to Equation 6:

$$\frac{KC}{R} = \left(\frac{1}{M_w} + 2A_2C\right) \times \left(1 + \frac{q^2 \cdot R_g^2}{3}\right) \qquad (6)$$

where A_2 is the second virial coefficient.

The refractive index increment (dn/dC) of the 4F-AZO-PEO molecule in water was measured using a differential refractometer Optilab rEX from Wyatt Technology Corporation and was found as (dn/dC) = 0.161 mL•g^{-1}. The same value of dn/dC was assumed for 2F2Cl-AZO-PEO.

Results are presented as mean ± standard deviation from the measured angles.

3. Results and discussion

The selection criteria for azobenzenes in this work were water-solubility, reversible photoswitching in the visible range, and relatively long-lived (day-scale half-life) *cis* forms. We explored two molecules expected to meet these criteria, each consisting of a tetra-*ortho*-substituted azobenzene head group bearing fluorine or chlorine atoms in the *ortho* positions and a short oligo(ethylene oxide) tail group attached in the *para* position.

3.1. Synthesis of azobenzene derivatives

Tetra-*ortho*-fluoro azobenzene poly(ethylene oxide) (4F-AZO-PEO) (7 EA units, MW = 580 g•mol^{-1}) was obtained from the synthesis platform of the Institut de chimie et biochimie moléculaires et supramoléculaires (ICBMS) in Lyon, following already described procedures.[14] The synthesis of dichloro difluoro azobenzene poly(ethylene oxide) (2Cl2F-AZO-PEO) (Scheme 1) starts with the commercially-available 3,5-dichloro-4-aminobenzoic acid, which was quantitatively esterified, followed by oxidation to nitrosoarene **2** using hydrogen peroxide in acetic and sulfuric acid at room temperature in a similar manner to Holmes *et al.*[42] A green solution characteristic of nitrosoarenes was obtained within 30 minutes, and after several hours a colourless crystalline precipitate started to form, corresponding to the more stable dimeric form of the nitrosoarene. Precipitation of the product avoids overoxidation by restricting contact with the oxidant.[42] The ^{1}H NMR spectrum of **2** shows a major peak at 8.14 ppm corresponding to the dimer and a minor peak at 8.10 ppm corresponding to the free nitrosoarene (Figure S1). Attempts to oxidise **1** in a 2-phase system using Oxone®, which has also been shown to limit overoxidation,[39] gave no reaction even upon heating due to the electron-poor nature of the aromatic system. The azobenzene photoswitch **3** was obtained in 48 % yield by Mill's reaction of **2** with 2,6-difluoroaniline using the approach developed by Knie *et al.*[39] ^{1}H NMR analysis showed a crude conversion of ca. 89 % with little byproduct formation (Figure S2).The yield of **3** could therefore likely be improved by optimizing the purification. Silica gel chromatography was performed with toluene as eluant, since TLC showed poorer separation in more traditional eluants based on EtOAc, (cyclo)hexane, and DCM; other eluants and/or polarity gradients may improve separation and increase isolated yield. Deprotection of the carboxyl group under basic conditions, followed by dicyclohexyl carbodiimide (DCC) coupling with HO–PEG$_8$–NH$_2$ gave 2Cl2F-AZO-PEO in overall yield of 30 %.
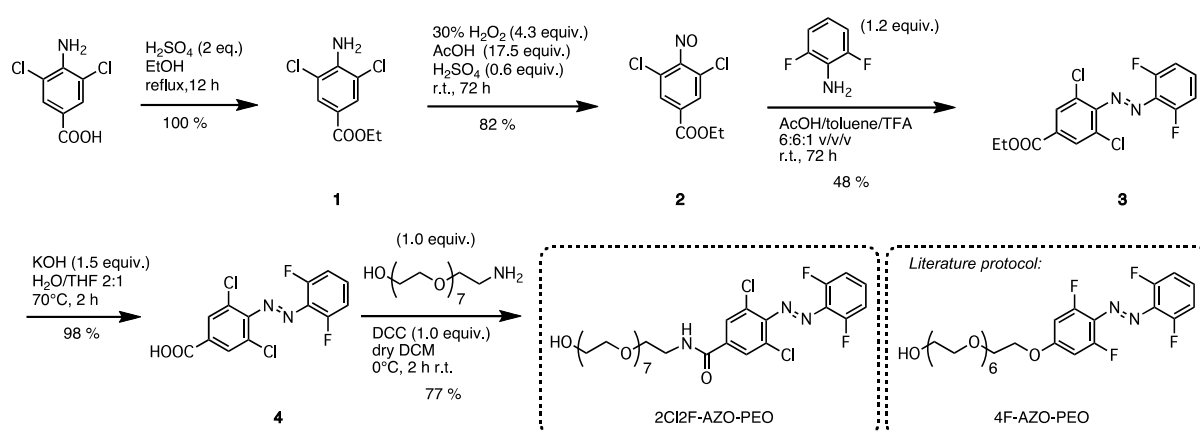
Scheme 1. Synthetic route for 2Cl2F-AZO-PEO, and the structure of 4F-AZO-PEO obtained according to the protocol reported by Huang et al.[14] The azobenzenes are drawn in their *trans* configurations.

Since the configuration of azobenzene species can influence self-assembly and complexation processes, *trans*-**4** was crystallized and analysed by XRD (Figure 1). The molecule crystallizes in the monoclinic space group P2$_1$/c. The phenyl rings are not coplanar, exhibiting a dihedral angle of 49.74(5)° and a C6-N1-N2-C7 torsion angle of -174.75(11)°. The C−N-N angles are C6-N1-N2 = 116.02(10)° and C7-N2-N1 = 110.40(10)°. In the crystal, there is an intermolecular hydrogen bond O-H⋯O with the distance O2⋯O1 = 2.635(2) Å and the angle O2-H2A-O1 = 178(2)°. The crystal packing shows π-π interactions between two parallel molecules with Cg1⋯Cg1 (-x, 1-y, 1-z) centroid-centroid distance of 3.720(2) Å, a perpendicular distance from the centroid Cg1 to the plane of the other ring of 3.391(1) Å and a slippage between the centroids of 1.529 Å. Cg1 is the centroid of C1−C6 phenyl rings. The non-coplanarity of the two aromatic rings has been observed for other tetra-*ortho*-azobenzenes bearing two *ortho*-chlorine atoms on the same aromatic ring and is attributed to steric effects.[40]
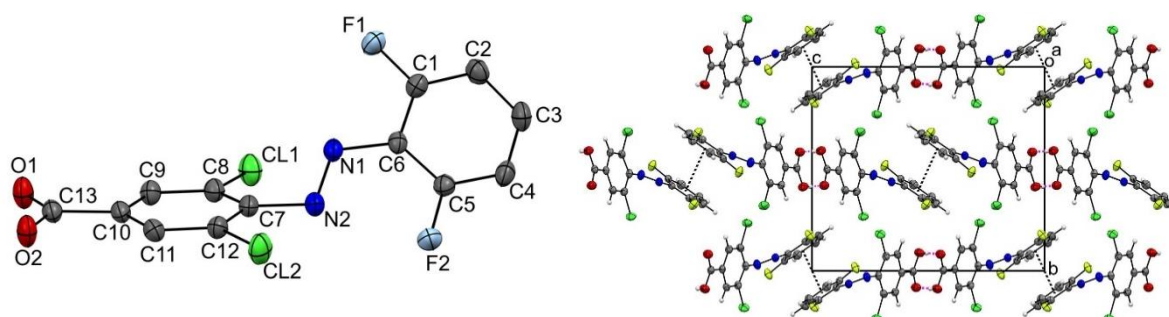
Figure 1. Molecular structure of **4** drawn with thermal ellipsoids at 50% probability level. Hydrogen atoms are omitted for clarity, and crystal packing of **4** viewed along the a axis. The black dashed lines indicate π-π interactions and the magenta dashed lines represent the hydrogen bond O-H⋯O.

3.2. Thermal relaxation of the *cis* forms

Photophysical properties were first explored in the new compound **3** to justify further studies in the PEG-conjugated derivative. The *cis*-rich photostationary state (PSS$_{cis}$) of **3** in deuterated acetonitrile was 86 % *cis* at 590 nm (by ^{1}H NMR spectroscopy), which shows the capacity of this azobenzene to reach relatively high *cis* enrichment using long visible wavelengths. Thermal relaxation studies performed by ^{1}H NMR spectroscopy in CD$_3$CN (Figure S6) showed *cis* thermal half-life ~4 days at room temperature and ~24 min at 70°C. Using this series of relaxation experiments at different temperatures, Arrhenius and Eyring plots provided the thermodynamic parameters for the thermal relaxation (Table S1), and allowed the half-life at 37 °C to be estimated as 19 h. The thermal relaxation is similar to that of tetra-*ortho*-chloro species and significantly faster than that of tetra-*ortho*-fluoro azobenzenes,[34] indicating that the chlorines detract from the strong *cis*-stabilizing effect imparted by the two fluorines. Nonetheless, a half-life of this order is appealing for some photopharmacological applications in which thermal reversion to the *trans* isomer on a days-timescale is desirable.[47]

The kinetics of thermal relaxation of PSS(530)$_{cis}$ 2Cl2F-AZO-PEO and PSS(365)$_{cis}$ 4F-AZO-PEO were assessed using UV-Visible spectroscopy (Figure 2 and Figures S7-S9). The expected exponential decrease is observed for all systems, together with a strong influence of the temperature. We found *cis*-2Cl2F-AZO-PEO and *cis*-4F-AZO-PEO to have high thermal stabilities in water, with half-lives of ~327 and ~390 days respectively at 25 °C. Although the stability of the compounds studied here is not as high as that of tetra-*ortho*-fluoro azobenzene,[32] it is strongly enhanced compared to precursor **3**, H-azobenzene, and 4Cl-AZO.[40] The corresponding activation energy barriers were found to be 127 kJ•mol^{-1} and 139 kJ•mol^{-1} for 4F-AZO-PEO and 2Cl2F-AZO-PEO respectively (Table 1). These energy values are very close to the one found for 4F-azobenzene in acetonitrile studied by Bléger *and coll.*[32] It seems that water does not significantly change the energy barrier of the thermal return compared to acetonitrile.
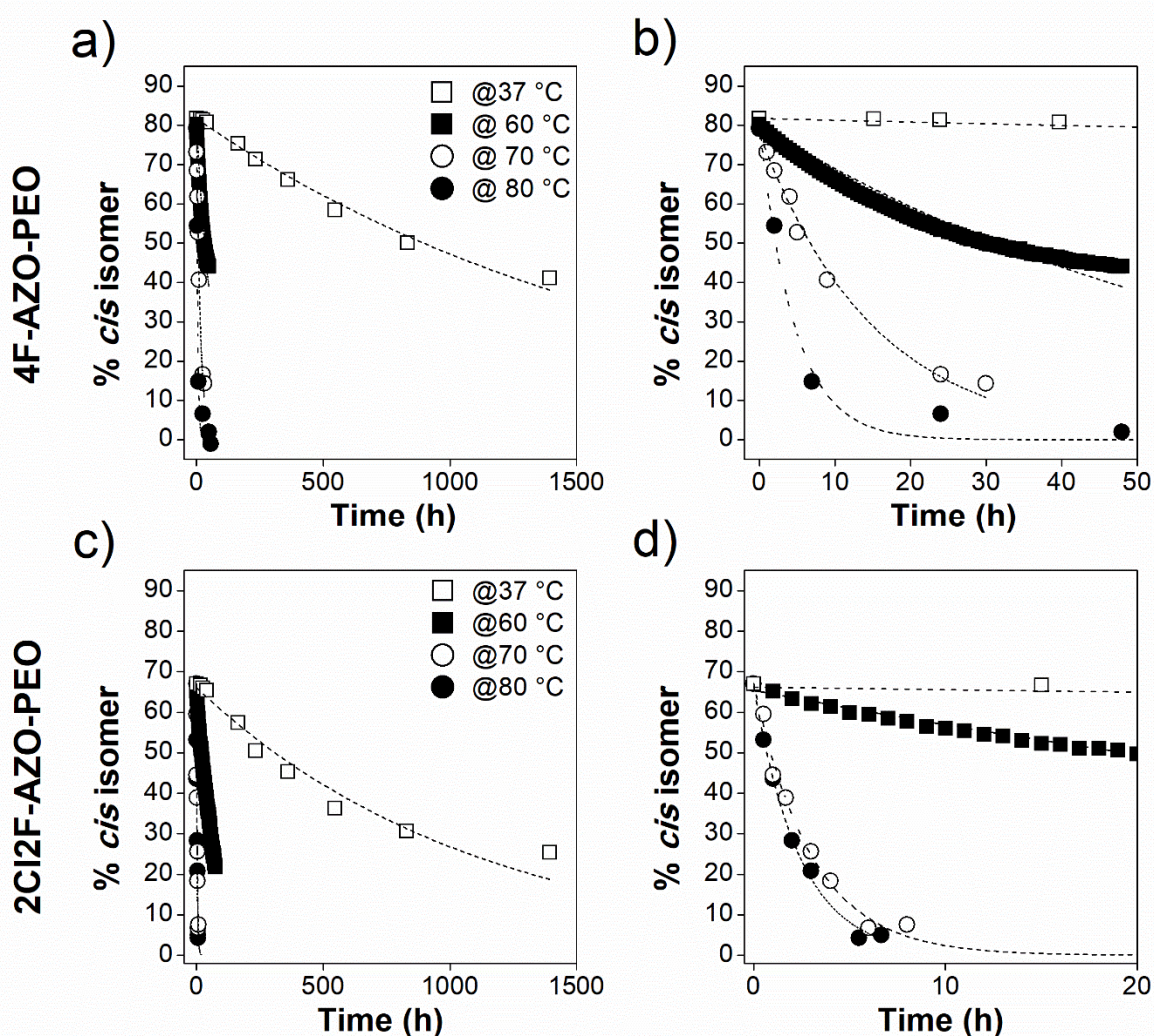
Figure 2. UV-Visible spectroscopy studies in water of the thermal relaxation in the dark at various temperatures of a) 4F-AZO-PEO (zoomed in b), and c) 2Cl2F-AZO-PEO (zoomed in d). The dotted lines correspond to the best first order exponential decay fit. Note that each series starts from the PSS$_{cis}$ achieved by irradiation with LEDs at 365 nm for 4F-AZO-PEO and 530 nm for 2Cl2F-AZO-PEO.

14

Table 1. Kinetic properties at 70 °C and thermodynamic properties of **3**, 2Cl2F-AZO-PEO and 4F-AZO-PEO compared with the 4F-azobenzene first synthesized by Bléger *et al.*[32]. [a] in CD$_3$CN, [b] in DMSO

	$\tau_{1/2}$ (days) 25°C*	k (s^{-1}) 70 °C	$\tau_{1/2}$ (h) 70 °C	A (s^{-1})	E_a (kJ•mol^{-1})	$\Delta H^\ddagger$ (kJ•mol^{-1})	$\Delta S^\ddagger$ (J•mol^{-1})	$\Delta G^\ddagger$ (kJ•mol^{-1})
3	4[a]	4.7·10^{-4}	0.41	2.9·10^{12}	104	101	-15	106
4F-azobenzene[32]	714[b]	5.4·10^{-6}	35.5	5.3·10^{11}	112	109	-28	117
2Cl2F-AZO-PEO	327	9.2·10^{-5}	2.09	4.8·10^{16}	139	136	65	113.5
4F-AZO-PEO	390	1.8·10^{-5}	10.5	3.9·10^{14}	127	124	25	116

3.3. Photoswitching of the azobenzene derivatives

The completeness of bidirectional photoswitching of both 4F-AZO-PEO and 2Cl2F-AZO-PEO under visible light was next investigated in water, which is a more relevant solvent for potential biological applications. Green light irradiation (530 nm, 30 mW•cm^{-2}, 15 min) of the dark-adapted compounds generated *cis*-enriched photostationary states, denoted PSS(530)$_{cis}$, with corresponding UV/Visible spectra shown in Figure 3a and b. The PSS(530)$_{cis}$ values for 4F-AZO-PEO and 2Cl2F-AZO-PEO were 72 % and 67 % *cis* respectively (^{1}H NMR, Figure 3c and d). Irradiation with blue light (415 nm, 90 mW•cm^{-2}, 5 min) led to PSS(415)$_{trans}$ values of 67 % and 83 % for 4F-AZO-PEO and 2Cl2F-AZO-PEO respectively (^{1}H NMR, Figure 3c and d). The PSS$_{cis}$ values are similar for each compound, as expected from the very similar absorption profiles at longer wavelengths ($\lambda > 500$ nm). In contrast, a much higher *trans* content at PSS(415)$_{trans}$ was attained for 2Cl2F-AZO-PEO (83 %) than for 4F-AZO-PEO (67 %), presumably due to the significantly higher absorption coefficient exhibited by the *cis* isomer of 2Cl2F-AZO-PEO in the blue region (400 – 450 nm) versus the *trans* isomer.
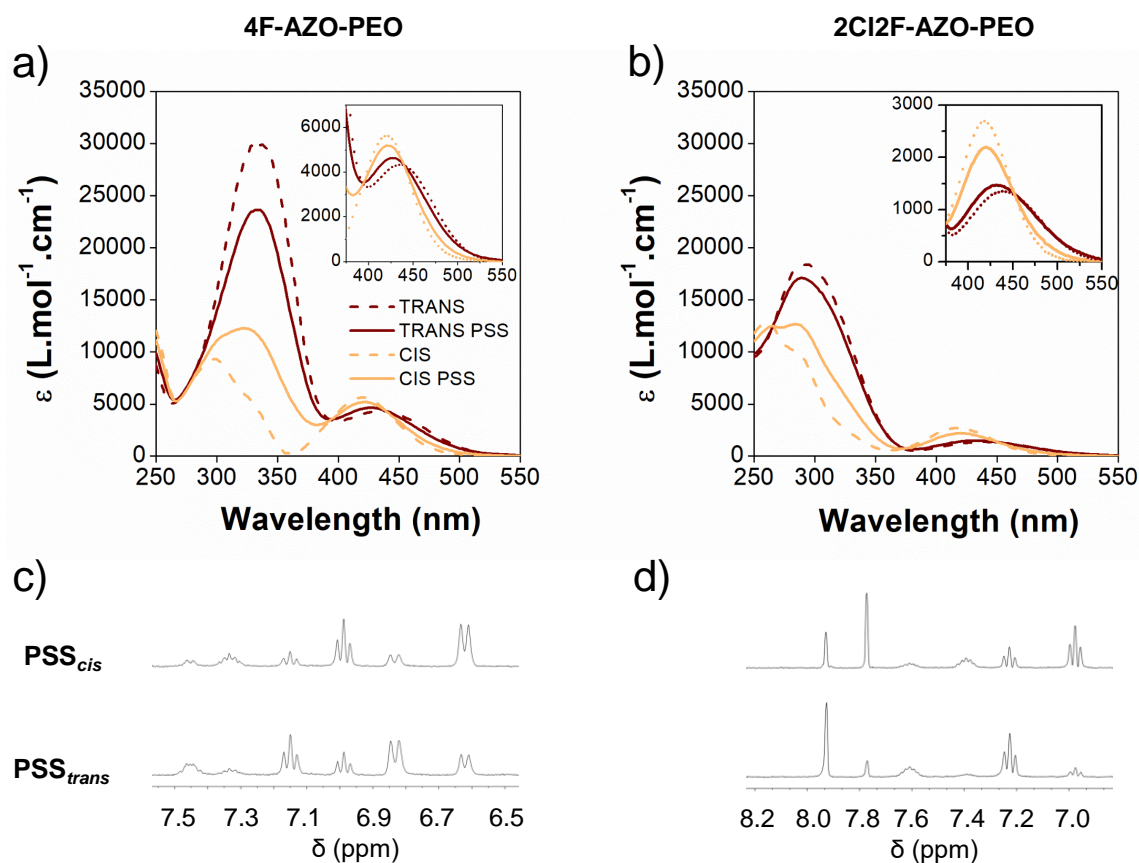
Figure 3. Absorption spectra in water of PSS(530)$_{cis}$ (orange solid lines) and PSS(415)$_{trans}$ (red solid lines) for a) 4F-AZO-PEO and b) 2Cl2F-AZO-PEO, with extrapolated spectra for the pure isomers shown as dotted lines. Partial ^{1}H NMR spectra focusing on the 6.5-8 ppm region of the c) 4F-AZO-PEO and d) 2Cl2F-AZO-PEO molecules at PSS(530)$_{cis}$ and PSS(415)$_{trans}$.

The quantification of the *cis/trans* ratio for both compounds allowed the calculation of the UV/Vis spectra of the pure *cis* and *trans* isomers of both compounds (Figure 3a, b). The positions, and therefore the separations, of the n→π* bands of each isomer were determined from these pure *cis* and *trans* spectra, and are summarized in Table 2.

Table 2. Maxima of the n$\rightarrow$ π* absorption band of *trans* and *cis* configurations of different azobenzene derivatives from the literature compared to 4F-AZO-PEO and 2Cl2F-AZO-PEO.

Compound	Solvent	Configuration	n$\rightarrow$π* λ_{max} (nm)	Reference
AZO	$CDCl_3$	*trans*	445	[48]
		cis	440	[25]
4F-AZO	CH_3CN	*trans*	458	[32]
		cis	416	[32]
4Cl-AZO	DMSO	*trans*	455	[40]
		cis	435	[40]
2Cl2F-AZO	DMSO	*trans*	460	[40]
		cis	420	[40]
4F-AZO-PEO	H_2O	*trans*	434	This work
		cis	420	
2Cl2F-AZO-PEO	H_2O	*trans*	440	This work
		cis	418	

The maximum of the n$\rightarrow$π* absorption band for 4F-AZO-PEO is 434 nm for pure *trans* and 420 nm for pure *cis*, corresponding to a separation of 14 nm. The n$\rightarrow$π* bands of the pure *trans* and *cis* isomers of 2Cl2F-AZO-PEO present a slightly higher separation of 22 nm. The factors affecting n$\rightarrow$π* separation in tetra-*ortho*-fluoro azobenzenes are well described in literature, [39] with symmetrical substitution of electron-withdrawing groups (EWGs) in *para* positions maximizing separation to ~ 50 nm, while mono-substitution and/or electron donating groups (EDGs)[49] in *para* positions decrease the separation by tens of nanometers. The presence of a single electron-donating ether group in the *para* position of our 4F-AZO-PEO is responsible for the modest n$\rightarrow$π* separation. Although the tetra-*ortho*-chloro substitution pattern has been shown to allow *trans-cis* isomerization at longer wavelengths than in tetra-*ortho*-fluoro analogues,[50] the n$\rightarrow$π* band separation is smaller (~ 24 nm in quantum mechanical computations for 4Cl-AZO [40]) which reduces completeness of *cis-trans* switching. In our 2Cl2F-AZO-PEO, we have two fluorines on one aromatic ring which is expected to promote n$\rightarrow$π* separation, but the mono-substitution in the para position, albeit with an EWG, disfavours n$\rightarrow$π* separation. Overall, the n$\rightarrow$π* separations and the PSS values exhibited by 4F-AZO-PEO and 2Cl2F-AZO-PEO are broadly consistent with expectations based on literature of related structures.

3.4. Host-guest complexes of azobenzene derivatives and β-CD

Azobenzene photoswitches are often employed to form light-controllable inclusion complexes, in particular with β-cyclodextrin (β–CD).[12, 51-55] The difference in geometry and polarity of the two azobenzene isomers encourages the formation of inclusion complexes with different association constants, typically with *trans* binding stronger than *cis*, and has been exploited in many high-tech applications such as light-sensitive smart materials.[12, 13] Most studies have nonetheless utilized UV-responsive azobenzenes in various solvents, with only a few papers

exploring tetra-*ortho*-substituted azobenzenes. Liao recently reported visible-light-responsive supramolecular gels formed in DMSO/H_2O 8/2 $_{v/v}$.[56] The system was comprised of β-cyclodextrin dimers mixed with tetra-*ortho*-methoxy azobenzene dimers, with the reversible sol-gel transition induced by self-assembly of supramolecular polymer chains formed upon *cis-trans* isomerization with blue light. Weng and co-workers formed inclusion complexes between carboxylated tetra-*ortho*-fluoro azobenzene and cyclodextrins in basic aqueous solutions,[57] showing that no inclusion complex was formed with α-CD, but that both *cis* and *trans* formed complexes with association constants in the 10^3 M^{-1} range and slightly higher binding for *cis* than *trans*. This preference of β-CD for the *cis* isomer was supported by Katsonis and Huskens using a tetra-*ortho*-fluoro azobenzene bearing PEO chains,[14] while Wu showed that hydrophilic tetra-*ortho*-methoxy azobenzenes exhibit the usual trend $K_{trans} > K_{cis}$.[58] The purpose of the present work was to determine the complexation behaviour of our new 2Cl2F-AZO-PEO in aqueous solution and benchmark it against that of 4F-AZO-PEO.

The formation of inclusion complexes between our *trans*-azobenzenes and β-CD was first studied in a classical manner by the shift of UV-Visible spectroscopy absorption bands (Figure S10) and ^{1}H NMR spectroscopy peaks (Figure S11) in the presence of β-CD. Upon addition of increasing amounts of β-CD, a modification of the UV-visible spectrum was observed and more markedly a shift in ^{1}H NMR spectroscopy of the aromatic protons of the molecules. These modifications are indicative of interactions between the aromatic protons and β-CD. This was also demonstrated by light scattering experiments for 4F-AZO-PEO (Figure S12), which showed a strong increase of the apparent molar mass of the scattering object upon addition of β-CD, as well as an increase of the hydrodynamic radius R_h from 5 to 40 nm.

Complexation of the two derivatives with β-CD was further characterized by determining i. the stoichiometry of the complexes formed by *trans*-rich and *cis*-rich solutions by Job plots (^{1}H NMR spectroscopy) and ii. the corresponding association constants by titration experiments using spectrophotometry. Job plots method was applied to all systems and tested with a polynomial equation corresponding to a complex at a ratio of 1:1. Job plots showing a maximum at β-CD mole fraction of 0.5 (Figure 4a, b and c) demonstrate that *trans*-rich and *cis*-rich 4F-AZO-PEO and the *trans*-rich 2Cl2F-AZO-PEO could complex the β-CD in 1:1 stoichiometry, as is a common [31, 57, 58].It is noteworthy that these Job plots were obtained on solutions for which the presence of the minor isomer was less than 15% (*cis*-rich 4F-AZO-PEO was obtained from irradiation at 366 nm leading to a PSS(365)$_{cis}$ at 86%). PSS(530)$_{cis}$ 2Cl2F-AZO-PEO, on the contrary, showed a small shift of the Job Plot curve with a peak at 0.4 (Figure 4d). A shift of the maximum is usually attributed to the presence of different stoichiometries or mixtures of different complexes, as Hibbert *et al.*[59] discussed. However, for this system, it is very unlikely that this corresponds to complexes in which more than one 2Cl2F-AZO-PEO is associated with the β-CD cavity due to the steric bulk of 2Cl2F-AZO. This system also contained the highest mole fraction of the minor isomer (33 % *trans*) which could have contributed to greater uncertainty in the obtained values. Conclusions that could be drawn for PSS(530)$_{cis}$ 2Cl2F-AZO-PEO are therefore limited, and we rather focused on determining the association constants for the other three systems.
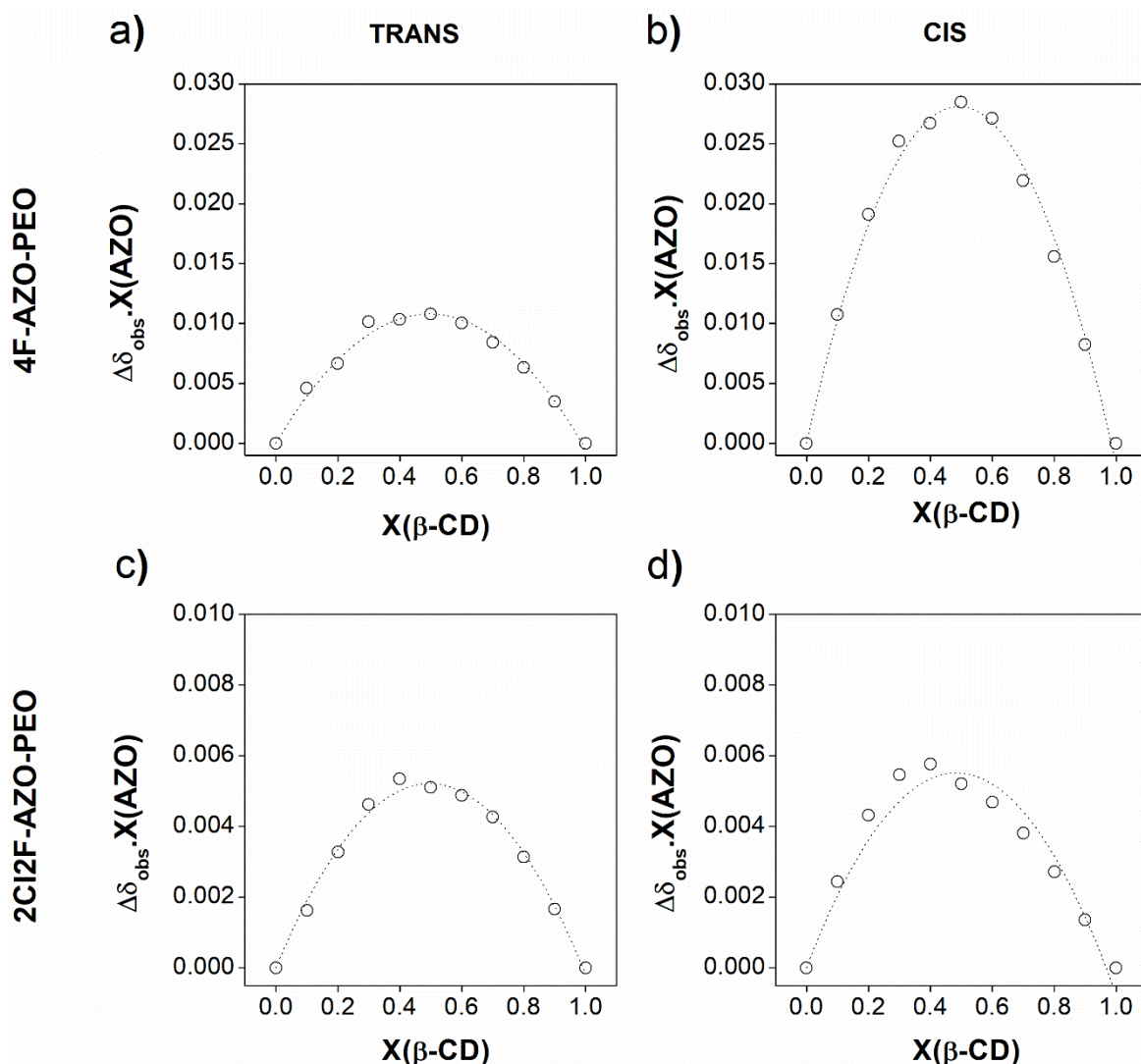
Figure 4. Job Plots of the complexes made between *β*-CD and a) *trans*-rich 4F-AZO-PEO (91 % *trans*), b) 4F-AZO-PEO at PSS(365)$_{cis}$ (86 % *cis*, obtained using 365 nm light irradiation), c) *trans*-rich 2Cl2F-AZO-PEO (83 % *trans*), and d) 2Cl2F-AZO-PEO at PSS(530)$_{cis}$ (67 % *cis*, obtained using 530 nm light irradiation). Open circles represent the experimental points and the full line the polynomial fit corresponding to a complex at a ratio of 1:1.

The association constants (Ka) were determined to assess whether light could be used to induce changes in the complexation strength between AZOs and β-CD (Figure S13 and Table 3). A Ka of 7120 M^{-1} for the PSS(365)$_{cis}$ rich-4F-AZO-PEO was found which is ca. 4.4 times higher than for its *trans*-rich state (1620 M^{-1}). The higher value for the PSS(365)$_{cis}$ than the *trans*-rich system agrees with the literature for such systems, but the difference that we obtained was larger than in the reported studies.[14, 57] Huskens and coll. found values of K$_a$ of 4800 and 2300 M^{-1} respectively for the *cis* and *trans* forms of a tetra-*ortho*-fluoroazobenzene with a long PEO chain,[14] with the mole fractions of the dominant isomers ≥ 90 %. Working with a tetra-*ortho*-fluoroazobenzene dicarboxylate in a bicarbonate solution, Weng and coll. found a very small difference in Ka between both forms (3000 and 2100 M^{-1} respectively for the *cis* and *trans* forms).[57] The authors showed by NMR that both *cis* and *trans* isomers of 4F-AZO inserted

in the cavity of β-CD from the secondary (larger) face, albeit with different spatial orientations. The driving forces for interaction in CD complexes are relatively weak non-specific interactions (Van der Waals, hydrophobic interactions, hydrogen bonding).[26] The *trans* form of 4F-AZO does not bind as strongly to β-CD as traditional *trans* azobenzenes, presumably because its non-planarity decreases interactions with the CD cavity compared with the planar orientation of traditional *trans* azobenzenes. In contrast, the *cis* form of 4F-AZO seems to favor interactions with the cavity, traditional *cis* azobenzenes do not interact. The large difference in affinity constants observed in our case for 4F-AZO-PEO shows that interesting photo-responsive properties could be expected for active systems incorporating both β-CD and this fluorinated azobenzene.

The K_a of the *trans*-rich 2Cl2F-AZO-PEO was found to be 330 M^{-1} which is 5-fold lower than that of 4F-AZO-PEO. The steric hindrance created by the two chlorine atoms and the tilted geometry shown in XRD presumably both hinder strong interaction between the azobenzene and the cyclodextrin. As previously mentioned, the stoichiometry of the complex involving *cis* 2Cl2F-AZO-PEO and β-CD could not be determined with certainty so neither could its Ka. Indeed, the ^{1}H NMR spectra performed for the Job plot clearly showed that both *trans* and *cis* forms were able to complex to β-CD, but this technique could not be used in a satisfactory manner to determine the association constant of each form, owing to high uncertainties of the maximum chemical shift. UV-visible spectroscopy could not be used as an alternative because of the overlap of the spectra from each isomer. Determining the association constant for *cis* 2Cl2F-AZO-PEO would constitute an entire study in itself, which was beyond the scope of this work. Nonetheless, the correlation between the shift in the aromatic proton signal in ^{1}H NMR and the strength of the complexation leads us to think that there is no significant difference between the binding affinities of the *trans*-rich and *cis*-rich 2Cl2F-AZO-PEO. We can conclude that the dichloro-difluoro azobenzene is too bulky to efficiently complex inside the β-CD cavity, compared to traditional and tetra-*ortho*-fluoro azobenzenes.

Table 3. Stoichiometry and association constants determined for azobenzene derivatives@β-CD complexes. The association constants have been determined for systems with 1:1 stoichiometry systems and fitted by numerical modeling (see SI). n.d. not determined

	4F-AZO-PEO *trans*-rich	4F-AZO-PEO *cis*-rich	2Cl2F-AZO –PEO *trans*-rich	2Cl2F-AZO-PEO *cis*-rich
Stoichiometry	1:1	1:1	1:1	n.d.
Ka (M^{-1})	1620	7120	330	n.d.

3.5. Self-assembly in aqueous solution

Although the β-CD complexation studies showed a modest photo-induced change in association constant for 4F-AZO-PEO, we hypothesized that interesting photoswitchable systems might be

attainable from the azobenzene derivatives alone. Both 4F-AZO-PEO and 2Cl2F-AZO-PEO exhibit amphiphilic characteristics coming from the combination of a short, water soluble PEO chain and a hydrophobic azobenzene moiety. These molecules are thus expected to self-assemble in a selective solvent such as water and this assembly might be influenced by geometric and polarity changes in the core azobenzene units.

Surface tension measurements were performed in order to determine the critical micelle concentration (CMC) of the two compounds at both PSS(415)$_{trans}$ and PSS(530)$_{cis}$. CMC values for both azo derivatives were estimated to ~ 1.5 mM irrespective to their configuration (Figure S14). The self-assembling behavior of the molecules was then investigated in water by static and dynamic light scattering (SLS and DLS) above their CMC and below their cloud point (Figure 5). The M_{app} and the hydrodynamic radius (R_h) are plotted as a function of the concentration for the two investigated species. Both oligomers form small micellar aggregates in water. For both species the apparent molar mass M_{app} did not show any angular dependence for all the concentrations studied regardless of their configuration, confirming the small size of the objects (R_g < 20 nm) in aqueous solution (Figure S15). 2Cl2F-AZO-PEO "micelles" exhibit a continuous increase in their M_{app} with increasing concentration regardless of the trans/cis configuration (Figure 5a). The evolution of R_h follows the same trend, ranging from 2 to 5 nm (Figure 5c). This assembly behavior is characteristic of an "open association" process in which the aggregation number (N_{agg}, defined as M_{app}/M_{unimer}) increases with concentration above the CMC.[60] Reversible switching from PSS(530)$_{cis}$ to PSS(415)$_{trans}$ states barely affects N_{agg} (~60 at 18 mM) and R_h (3 nm) of 2F-2Cl-AZO-PEO self-assemblies. 4F-AZO-PEO exhibits a more peculiar behavior. Within the experimental error, the PSS(415)$_{trans}$ 4F-AZO-PEO did not show any concentration dependence of M_{app} (averaged N_{agg} ~ 170) (Figure 5b). This behavior is characteristic of a "closed association" mechanism in which N_{agg} remains constant with concentration once the CMC is reached.[60] Surprisingly, upon irradiation with green light, the PSS(530)$_{cis}$ 4F-AZO-PEO form showed an increase in M_{app} (N_{agg} increased from 30 to 1 000) and an increase in R_h (from 4 to 11 nm) with increasing concentration (Figure 5b and 5d). Thus, it exhibits an open association behavior in the *cis* configuration. The self-association process (open or closed association) of 4F-AZO-PEO therefore differs depending on the configuration of the 4F-AZO group. Increasing the temperature up to their respective cloud points induces an increase of M_{app} and R_h of both 2Cl2F-AZO-PEO and 4F-AZO-PEO (Figure S16). However, this effect remains moderate and the aggregates probably do not undergo morphological transition before they phase separate at the cloud point.

To the best of our knowledge, the self-associating behavior of analogous PEO oligomers bearing a traditional azobenzene moiety at the chain-end has not been reported. Tabor et al.[61] reported the synthesis and characterization of nonionic azobenzene-containing photosurfactants. The morphology of the micelles strongly depended on the nature of the sugar unit (from spherical to worm-like micelles) but in all the cases, photoisomerization from *trans* to *cis* always led to smaller micelles that sometimes completely disassociated. According to SANS measurements, Tabor et al.[61] also suggested that the *cis* isomers packed more closely giving thinner elongated micelles exhibiting lower N_{agg}. The behavior of halogenated-AZO-PEO is quite different. Renou et al.[62] showed that PEO-C12 associated according to an open

association mechanism whereas PEO-C18 exhibited a closed association mechanism. An increase of hydrophobicity therefore seemed to favor the closed association mechanism. In our work, both forms of 2Cl2F-AZO moiety are moderately hydrophobic, leading to an open association mechanism while the more planar (and therefore more apolar) *trans* configuration of 4F-AZO would be the most hydrophobic of the four species, leading to a self-assembly according to a closed association mechanism. However, the *cis* form of 4F-AZO showed both an open association mechanism and strong aggregation, which cannot be explained by its moderate hydrophobicity alone. We speculate that 4F-AZO-PEO in *cis* configuration tends to adopt a micellar organization favoring higher aggregation numbers as the concentration increases. The peculiar photo-responsive association mechanism of 4F-AZO-PEO has not been reported in the literature and it opens interesting perspective for controlled release applications.
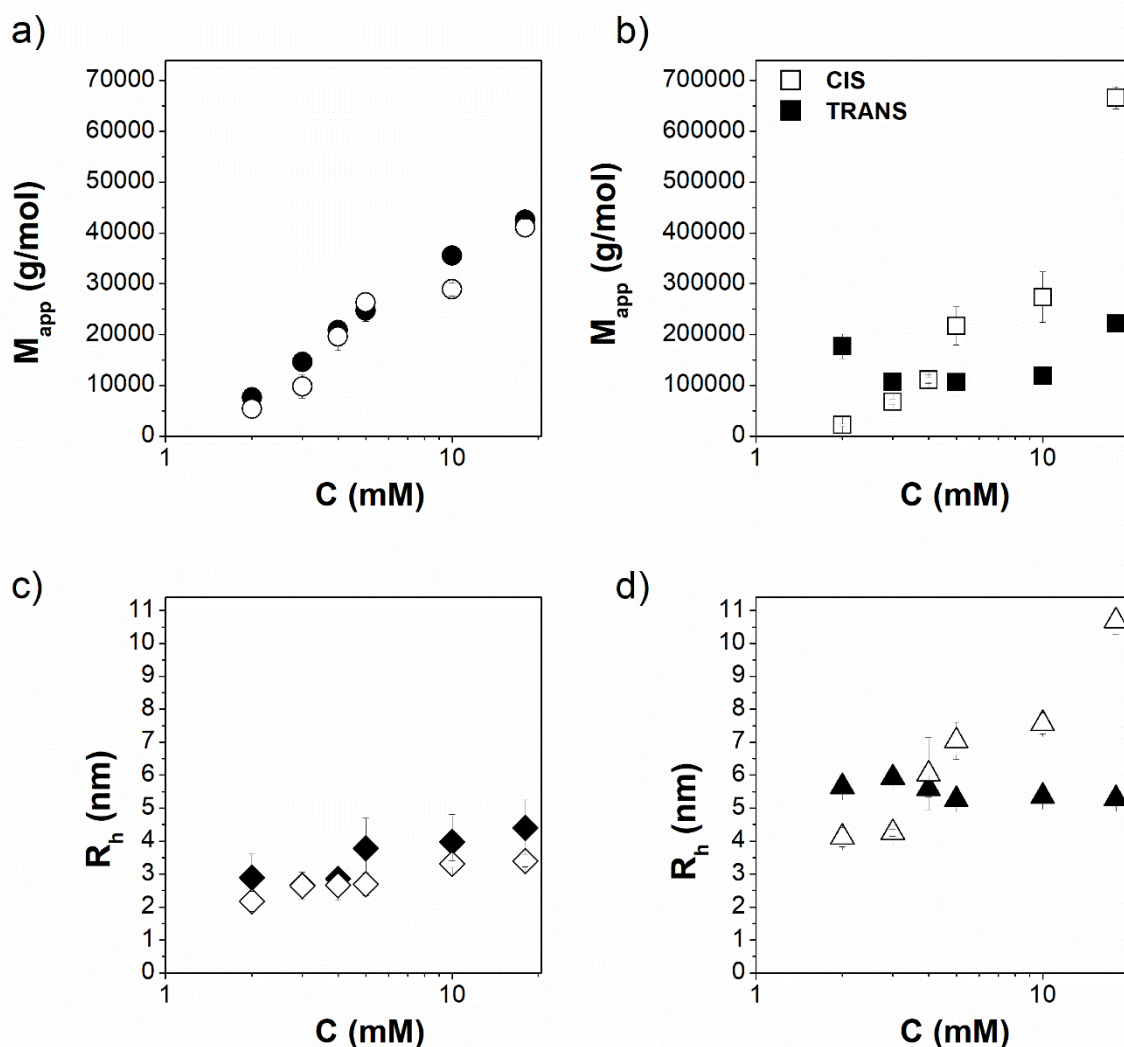
Figure 5. Apparent molar masses of a) 2Cl2F-AZO-PEO and b) 4F-AZO-PEO aqueous assemblies and the corresponding hydrodynamic radii for c) 2Cl2F-AZO-PEO and d) 4F-AZO-PEO as a function of concentration and isomerization state, where filled symbols refer to PSS(415)*trans* and open symbols refer to PSS(530)*cis*. Results are presented as mean ± standard deviation from the measured angles.

3.6. Lower Critical Solution Temperature in aqueous solution

Both 4F-AZO-PEO and 2Cl2F-AZO-PEO molecules at PSS(530)$_{cis}$ and PSS(415)$_{trans}$ exhibit a cloud point (CP) in aqueous solution (see for instance Figure 6a), indicative of the formation of aggregates of a size in the visible range. CP values of both oligomers were determined using turbidity measurements (Figure S17). 4F-AZO-PEO exhibits a CP between 10 and 28°C while the CP of 2Cl2F-AZO-PEO is higher (between 45 and 50 °C) for the concentration range studied (2-10 mM) (Figure 6b). This difference seems to indicate a lower hydrophobicity of the 2Cl2F-AZO moiety compared to the 4F-AZO one, which is supported by their self-assembling behavior observed in the previous section. The CP of 2Cl2F-AZO-PEO decreases with increasing concentration, as observed in other systems such as poly(*N*-isopropylacrylamide) in water. [63] The 4F-AZO-PEO exhibits a minimum of CP at 5 mM which can be considered as the lower critical solution temperature (LCST). A shift of LCST upon *cis/trans* conversion is expected, as already reported for many (co)polymers bearing traditional azobenzenes and dissolved in water[64-69] or in ionic liquids.[70, 71] Generally, the *cis* form exhibits higher LCST value than the *trans* one due to the lower hydrophobicity (higher dipole moment) of the azobenzene group in *cis* configuration.
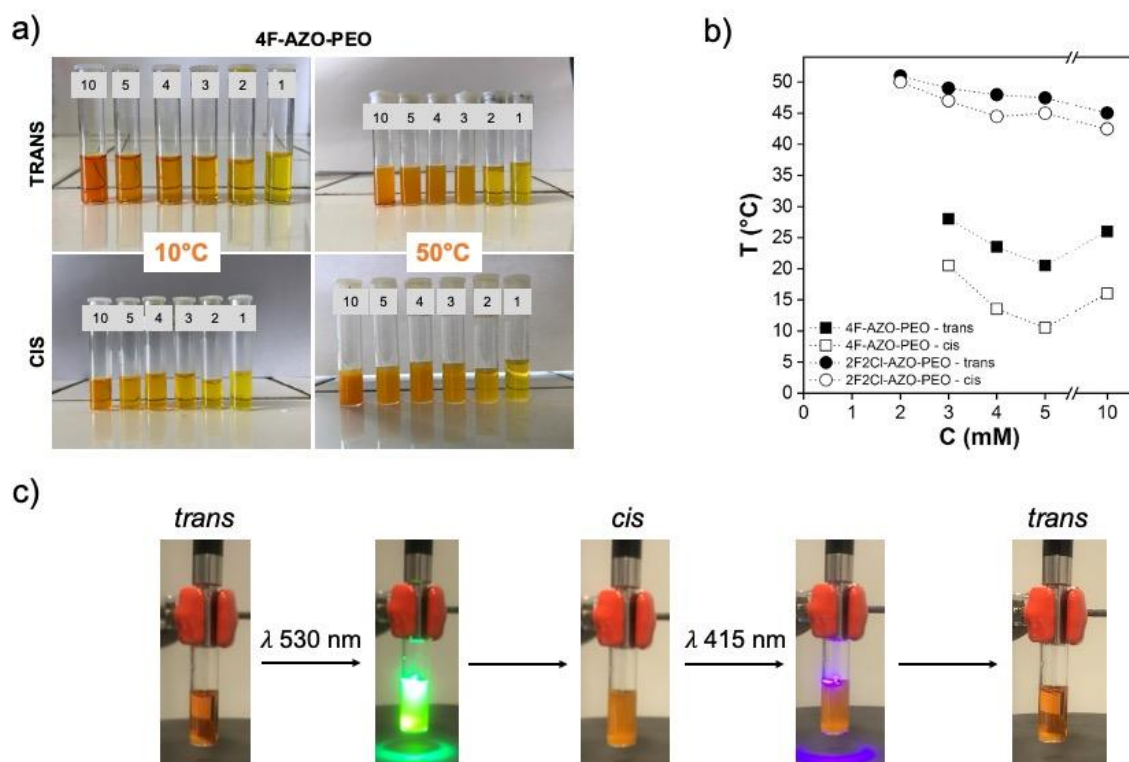
Figure 6. a) Pictures of the 4F-AZO-PEO in aqueous solutions at 10 °C (left) and 50 °C (right) in PSS(415)$_{trans}$ (top) and PSS(530)$_{cis}$ (bottom) configuration. The number labels refer to the concentration of the solutions in mM b) Concentration dependence of the cloud point of 2F2Cl-AZO-PEO (■) and 4F-AZO-PEO (□) in the *cis*-rich (open symbols) and *trans*-rich (closed symbols) forms. c) Pictures of reversible photoswitching of 4F-AZO-PEO at 10 mM at room temperature following visible light irradiation.

Unexpectedly, CP values of both 4F-AZO-PEO and 2F-2Cl-AZO-PEO in the *cis*-rich system are lower than in the *trans*-rich one (although the LCST values of the 2Cl2F compound are very close in both configurations). This phenomenon cannot be explained by a lower dipole moment (and therefore increased hydrophobicity) of the *cis* form of 4F-AZO group compared to the *trans* one, since Zhao *et al.*[72] observed and computed the inverse. The purifications of our azobenzenes using silica gel chromatography also showed higher polarity (lower Rf values) for the *cis* isomers. As shown before, the self-assembly behavior of 4F-AZO-PEO does not simply rely on the hydrophobicity of the AZO group but the origin of this unexpected observation in LCST values remains unclear.

The difference of LCST between the PSS(530)*cis* and PSS(415)*trans* forms of 4F-AZO-PEO confers light-responsive properties to the solution transparency. A turbid solution (C = 10 mM) can be reversibly rendered limpid by triggering the *cis* to *trans* switch of the azo moieties using blue light irradiation (or inversely green light) at room temperature (Figure 6c). Such photoswitchable aggregation/dissolution has been investigated in traditional azobenzene-containing polymeric systems intended as smart delivery materials,[73] aggregation-induced fluorescent probes,[74] logic circuits,[75] and nanoparticle absorption modulators for sensing/therapy.[76] These reports[73-78] of traditional azobenzene assemblies used for various applications, including biology, rely on UV light even though the risk of UV light to cells is well known.[28] The few reports of visible-switchable azobenzene complexes[14, 57] show smaller differences in binding constants of *cis* and *trans* with β-CD than in this work, and do not explore self-assembly behavior of the azobenzene species itself. A summary showing key features of literature reports in relation to the present work is provided in Table 4. Our results show that 4F-AZO-PEO is a good candidate for achieving similar functions with all-visible light switchability.

Conclusion

In this work, the tetra-*ortho*-fluoro substituted azobenzene 4F-AZO-PEO was shown to undergo reversible complexation with β-cyclodextrin (β-CD) and reversible self-assembly in water driven by all-visible photoswitching. The half-life of the *cis* isomer was > 300 days at room temperature, offering very high thermal stability that supports bidirectional switching with light. The *cis* form of 4F-AZO-PEO showed a binding constant with β-CD that was 4.4 times higher than that of the *trans* form. This is larger than the 1.4- and 2.1-fold differences reported in literature for related systems, [14, 57] and could be significant enough to drive reversible assemblies for self-healing materials or photopharmacology in future work.[13, 18, 27, 53] The amphiphilic nature of 4F-AZO-PEO also encouraged self-assembly in water. Solutions above the critical micelle concentration showed LCSTs in water, with a large gap of ca. 10 °C between the cloud points for *cis* and *trans* states facilitating photoreversible aggregation at around room temperature using visible light. For comparison, a new dihloro-

difluoro-substituted azobenzene 2Cl2F-AZO-PEO was also synthesized and showed *cis* half-life > 300 days at room temperature, but lower β-CD binding constant and only modest differences in self-assembly upon photoswitching were attained.

As discussed before, the ability to drive 4F-AZO-PEO complexation and self-assembly above and below its cloud point using visible light in water advances the field of photodissociable systems by offering full aqueous solubility, all-visible photoswitching, high *cis* stability, and well-separated cloud points that straddle room temperature. The abundant reports [73-78] of traditional azobenzene assemblies used for various applications, including biology, rely on UV light even though the risk of UV light to cells is well known.[28] The few reports of visible-switchable azobenzene complexes[14, 57] show smaller differences in binding constants of *cis* and *trans* with β-CD than in this work, and do not explore self-assembly behavior of the azobenzene species itself. These are summarized in Table 4. The present work shows that 4F-AZO-PEO is suitable for designing all-visible-responsive smart materials that utilize its reversible complexation with β-CD and self-assembly at ambient temperature in water. Future work will focus on shifting the LCSTs to straddle body temperature for reversible aggregation under physiological conditions, and explore aggregation behaviour in the presence of therapeutic payloads and sensing species.

Table 4. Summary of relevant azobenzene-based complexation and self-assembly systems compared to the work presented here.

System	Azobenzene type	Envisaged application	Switching wavelengths	Solvent	Relevance to the present work	Ref.
Azobenzene-substituted polyethyleneimine	Traditional	Drug delivery	357 nm / 440 nm	Water	▪ 35 °C shift in LCST with photoisomerisation ▪ Required UV light	[73]
PEG-azobenzene block copolymers	Traditional (EDG in *para*)	Aggregation-induced fluorescent probes	450 nm / thermal relaxation	Water	▪ Self-assembled vesicles with aggregation-induced emission ▪ Visible *trans-cis* isomerisation accompanied by short *cis* lifetime (< 1.5 h)	[74]
Azobenzene-terminated polymer complexed with β-CD dimers	Traditional	Logic circuits	365 nm / 254 nm	Water	▪ Isomerisation-driven LCST shift of 2 °C ▪ Required UV light	[75]
AuNPs coated with azobenzene-decorated polymer	Traditional	Nanoparticle aggregation for sensing/therapy	354 nm / 440 nm	Water	▪ Isomerisation-driven LCST shift of 14 °C (polymer only) ▪ Required UV light	[76]

Self-aggregating azobenene-bearing polypeptide	Traditional	Fundamental study	365 nm / > 500 nm	Water/EtOH	▪ Water/EtOH mixture as solvent ▪ Required UV light	[78]
Azobenzene/DNA complexes	Traditional	Photoreversible nanostructures and particle assemblies	365 nm / 440 nm	Water	▪ Photoswitchable aggregates in water ▪ Required UV light	[77]
4F-AZO-PEG/β-CD complexes	Tetra-*ortho*-fluoro substituted	Host-guest supramolecular systems	365 nm / 420 nm	Water	▪ Longer PEG chain than in this work ▪ 2.1-fold higher binding constant for *cis* isomer vs. *trans* isomer ▪ All-visible photoswitching capacity not exploited	[14]
4F-AZO-COOH/β-CD complexes	Tetra-*ortho*-fluoro substituted	Host-guest supramolecular systems	540 nm / 440 nm	Water	▪ 1.4-fold higher binding constant for *cis* isomer ▪ Reliance on deprotonation of the COOH group for water solubility	[57]
4F-AZO-PEG/β-CD complexes and self-assemblies	Tetra-*ortho*-fluoro substituted	Drug delivery and sensing	540 nm / 440 nm	Water	▪ 4.4-fold higher binding constant for *cis* isomer ▪ Isomerisation-driven LCST shift of 10 °C allowing visible-driven (dis)assembly at room temperature	This work

EDG = electron-donating group. PEG = poly(ethylene glycol)

Supplementary information

NMR characterization of the new products, fitting details for thermal stability, complexation with b-CD, details on surface tension, light scattering and turbidimetry experiments. Movie showing the clear/turbid switch of 4F-AZO-PEO solutions under blue and green light.

Author Contributions

C. Courtine investigation, validation and writing-original draft, I. Hamouda, investigation, validation and writing-original draft, S. Pearson investigation, methodology, writing-original draft, L. Billon supervision, P. Lavedan investigation, S. Ladeira investigation, J.-C. Micheau investigation, V. Pimienta investigation, E. Nicol conceptualization, methodology, supervision

and writing-review and editing, N. Lauth de Viguerie conceptualization, methodology, supervision, writing-review and editing, and A.-F. Mingotaud conceptualization, methodology, funding acquisition, supervision and writing-review and editing. All authors contributed to the writing of the original draft

Conflicts of interest

There are no conflicts to declare.

Acknowledgements

References

[1] W. Wang, X. Lv, J.L. Moran, S. Duan, C. Zhou, A practical guide to active colloids: choosing synthetic model systems for soft matter physics research, Soft Matter, 16 (2020) 3846-3868, 10.1039/D0SM00222DI.

[2] L.W. Giles, C.F.J. Faul, R.F. Tabor, Azobenzene isomerization in condensed matter: lessons for the design of efficient light-responsive soft-matter systems, Materials Advances, 2 (2021) 4152-4164, 10.1039/D1MA00340BI.

[3] S. Chen, R. Costil, F.K.-C. Leung, B.L. Feringa, Self-Assembly of Photoresponsive Molecular Amphiphiles in Aqueous Media, Angewandte Chemie International Edition, 60 (2021) 11604-11627, https://doi.org/10.1002/anie.202007693I.

[4] M. Zhu, H. Zhou, Azobenzene-based small molecular photoswitches for protein modulation, Organic & Biomolecular Chemistry, 16 (2018) 8434-8445, 10.1039/C8OB02157KI.

[5] H.-B. Cheng, S. Zhang, J. Qi, X.-J. Liang, J. Yoon, Advances in Application of Azobenzene as a Trigger in Biomedicine: Molecular Design and Spontaneous Assembly, Advanced Materials, 33 (2021) 2007290, https://doi.org/10.1002/adma.202007290I.

[6] P.-F. Luo, S.-L. Xiang, C. Li, M.-Q. Zhu, Photomechanical polymer hydrogels based on molecular photoswitches, Journal of Polymer Science, 59 (2021) 2246-2264, https://doi.org/10.1002/pol.20210567I.

[7] A. Goulet-Hanssens, C.J. Barrett, Photo-control of biological systems with azobenzene polymers, Journal of Polymer Science Part A: Polymer Chemistry, 51 (2013) 3058-3070, https://doi.org/10.1002/pola.26735I.

[8] J. Groppi, M. Baroncini, M. Venturi, S. Silvi, A. Credi, Design of Photo-Activated Molecular Machines: Highlights from the Past Ten Years, Chemical Communications, 55 (2019) 12595-12602, https://doi.org/10.1039/C9CC06516DI.

[9] E.R. Kay, D.A. Leigh, Rise of the Molecular Machines, Angewandte Chemie International Edition, 54 (2015) 10080-10088, https://doi.org/10.1002/anie.201503375I.

[10] S. Shinkai, T. Nakaji, Y. Nishida, T. Ogawa, O. Manabe, Photoresponsive crown ethers. 1. Cis-trans isomerism of azobenzene as a tool to enforce conformational changes of crown ethers and polymers, Journal of the American Chemical Society, 102 (1980) 5860-5865, 10.1021/ja00538a026I.

[11] M. Salzano de Luna, V. Marturano, M. Manganelli, C. Santillo, V. Ambrogi, G. Filippone, P. Cerruti, Light-responsive and self-healing behavior of azobenzene-based supramolecular hydrogels, Journal of Colloid and Interface Science, 568 (2020) 16-24, https://doi.org/10.1016/j.jcis.2020.02.038I.

[12] D. Wang, W. Zhao, Q. Wei, C. Zhao, Y. Zheng, Photoswitchable Azobenzene/Cyclodextrin Host-Guest Complexes: From UV- to Visible/Near-IR-Light-Responsive Systems, ChemPhotoChem, 2 (2018) 403-415, 10.1002/cptc.201700233I.

[13] M. Mohamadhoseini, Z. Mohamadnia, Supramolecular self-healing materials via host-guest strategy between cyclodextrin and specific types of guest molecules, Coordination Chemistry Reviews, 432 (2021) 213711, https://doi.org/10.1016/j.ccr.2020.213711I.

[14] H. Huang, A. Juan, N. Katsonis, J. Huskens, Competitive inclusion of molecular photo-switches in host cavities, Tetrahedron, 73 (2017) 4913-4917, https://doi.org/10.1016/j.tet.2017.05.026I.

[15] L. Zou, C.J. Addonizio, B. Su, M.J. Sis, A.S. Braegelman, D. Liu, M.J. Webber, Supramolecular Hydrogels via Light-Responsive Homoternary Cross-Links, Biomacromolecules, 22 (2021) 171-182, 10.1021/acs.biomac.0c00950I.

[16] A. Samanta, B.J. Ravoo, Metal Ion, Light, and Redox Responsive Interaction of Vesicles by a Supramolecular Switch, Chemistry – A European Journal, 20 (2014) 4966-4973, https://doi.org/10.1002/chem.201304658I.

[17] J. Blass, B.L. Bozna, M. Albrecht, J.A. Krings, B.J. Ravoo, G. Wenz, R. Bennewitz, Switching adhesion and friction by light using photosensitive guest–host interactions, Chemical Communications, 51 (2015) 1830-1833, 10.1039/C4CC09204JI.

[18] J. Royes Mir, C. Coudret, C. Roux, F. Benoit-Marquié, M. Cazalès, C. Séverac, C. Lorenzo, A.-F. Mingotaud, Rational Hydrogel Formulation Leads to Reversible and Enhanced Photocontrolled Rigidity, ChemPhotoChem, 1 (2017) 311-316, 10.1002/cptc.201700038I.

[19] E.M. Nehls, A.M. Rosales, K.S. Anseth, Enhanced user-control of small molecule drug release from a poly(ethylene glycol) hydrogel via azobenzene/cyclodextrin complex tethers, Journal of Materials Chemistry B, 4 (2016) 1035-1039, 10.1039/C5TB02004BI.

[20] Y. Wang, G. Wang, Y. Ni, J. Zhou, S. Wang, Y. Gu, D. Zhang, S.Y. Zheng, Z.L. Wu, Q. Zheng, J. Zheng, J. Yang, Dual-Responsive Supramolecular Antimicrobial Coating Based on Host-Guest Recognition, Advanced Materials Interfaces, n/a (2022) 2201209, https://doi.org/10.1002/admi.202201209I.

[21] Q. Bian, W. Wang, S. Wang, G. Wang, Light-Triggered Specific Cancer Cell Release from Cyclodextrin/Azobenzene and Aptamer-Modified Substrate, ACS Applied Materials & Interfaces, 8 (2016) 27360-27367, 10.1021/acsami.6b09734I.

[22] Z. Ye, Y. Wang, S. Liu, D. Xu, W. Wang, X. Ma, Construction of Nanomotors with Replaceable Engines by Supramolecular Machine-Based Host–Guest Assembly and Disassembly, Journal of the American Chemical Society, 143 (2021) 15063-15072, 10.1021/jacs.1c04836I.

[23] S. Pearson, J. Feng, A. del Campo, Lighting the Path: Light Delivery Strategies to Activate Photoresponsive Biomaterials In Vivo, Adv. Funct. Mater., 31 (2021), 10.1002/adfm.202105989, 2105989I.

[24] D. Samanta, J. Gemen, Z. Chu, Y. Diskin-Posner, L.J.W. Shimon, R. Klajn, Reversible photoswitching of encapsulated azobenzenes in water, Proceedings of the National Academy of Sciences, 115 (2018) 9379-9384, 10.1073/pnas.1712787115I.

[25] H.M.D. Bandara, S.C. Burdette, Photoisomerization in different classes of azobenzene, Chemical Society Reviews, 41 (2012) 1809-1825, 10.1039/C1CS15179GI.

[26] A.M. Sanchez, R.H. de Rossi, Effect of β-Cyclodextrin on the Thermal Cis–Trans Isomerization of Azobenzenes., Journal of Organic Chemistry, 61 (1996) 3446-3451,

[27] J. Royes, C. Courtine, C. Lorenzo, N. Lauth-de Viguerie, A.-F. Mingotaud, V. Pimienta, Quantitative Kinetic Modeling in Photoresponsive Supramolecular Chemistry: The Case of Water-Soluble Azobenzene/Cyclodextrin Complexes, The Journal of Organic Chemistry, 85 (2020) 6509-6518, 10.1021/acs.joc.0c00461I.

[28] F.A. Jerca, V.V. Jerca, R. Hoogenboom, Advances and opportunities in the exciting world of azobenzenes, Nature Reviews Chemistry, 6 (2022) 51-69, 10.1038/s41570-021-00334-wI.

[29] A.A. Beharry, O. Sadovski, G.A. Woolley, Azobenzene Photoswitching without Ultraviolet Light, Journal of the American Chemical Society, 133 (2011) 19684-19687, 10.1021/ja209239mI.

[30] S. Samanta, T.M. McCormick, S.K. Schmidt, D.S. Seferos, G.A. Woolley, Robust visible light photoswitching with ortho-thiol substituted azobenzenes, Chemical Communications, 49 (2013) 10314-10316, 10.1039/C3CC46045BI.

[31] D. Wang, M. Wagner, A.K. Saydjari, J. Mueller, S. Winzen, H.-J. Butt, S. Wu, A Photoresponsive Orthogonal Supramolecular Complex Based on Host–Guest Interactions, Chemistry – A European Journal, 23 (2017) 2628-2634, https://doi.org/10.1002/chem.201604634I.

[32] D. Bléger, J. Schwarz, A.M. Brouwer, S. Hecht, o-Fluoroazobenzenes as Readily Synthesized Photoswitches Offering Nearly Quantitative Two-Way Isomerization with Visible Light, Journal of the American Chemical Society, 134 (2012) 20597-20600, 10.1021/ja310323yI.

[33] L.N. Lameijer, S. Budzak, N.A. Simeth, M.J. Hansen, B.L. Feringa, D. Jacquemin, W. Szymanski, General Principles for the Design of Visible-Light-Responsive Photoswitches: Tetra-ortho-Chloro-Azobenzenes, Angewandte Chemie International Edition, 59 (2020) 21663-21670, https://doi.org/10.1002/anie.202008700I.

[34] S. Samanta, A.A. Beharry, O. Sadovski, T.M. McCormick, A. Babalhavaeji, V. Tropepe, G.A. Woolley, Photoswitching Azo Compounds in Vivo with Red Light, Journal of the American Chemical Society, 135 (2013) 9777-9784, 10.1021/ja402220tI.

[35] Q. Bian, S. Chen, Y. Xing, D. Yuan, L. Lv, G. Wang, Host-guest self-assembly toward reversible visible-light-responsive switching for bacterial adhesion, Acta Biomaterialia, 76 (2018) 39-45, https://doi.org/10.1016/j.actbio.2018.06.039I.

[36] S. Passlick, M.T. Richers, G.C.R. Ellis-Davies, Thermodynamically Stable, Photoreversible Pharmacology in Neurons with One- and Two-Photon Excitation, Angewandte Chemie, 130 (2018) 12734-12737,

[37] K. Kumar, C. Knie, D. Bléger, M.A. Peletier, H. Friedrich, S. Hecht, D.J. Broer, M.G. Debije, A.P.H.J. Schenning, A chaotic self-oscillating sunlight-driven polymer actuator, Nature communications, 7 (2016) 11975, 10.1038/ncomms11975I.

[38] M.J. Hansen, M.M. Lerch, W. Szymanski, B.L. Feringa, Direct and Versatile Synthesis of Red-Shifted Azobenzenes, Angewandte Chemie International Edition, 55 (2016) 13514-13518, https://doi.org/10.1002/anie.201607529I.

[39] C. Knie, M. Utecht, F. Zhao, H. Kulla, S. Kovalenko, A.M. Brouwer, P. Saalfrank, S. Hecht, D. Bléger, ortho-Fluoroazobenzenes: Visible Light Switches with Very Long-Lived Z Isomers, Chemistry – A European Journal, 20 (2014) 16492-16501, 10.1002/chem.201404649I.

[40] D.B. Konrad, G. Savasci, L. Allmendinger, D. Trauner, C. Ochsenfeld, A.M. Ali, Computational Design and Synthesis of a Deeply Red-Shifted and Bistable Azobenzene, Journal of the American Chemical Society, 142 (2020) 6538-6547, 10.1021/jacs.9b10430I.

[41] S. Lv, X. Li, L. Yang, H. Ren, J. Jiang, Computational design of photoswitchable anion receptors: Red-shifted and bistable di-ortho-fluoro di-ortho-chloro azobenzene derivatives, Chemical Physics, 548 (2021) 111246, https://doi.org/10.1016/j.chemphys.2021.111246I.

[42] R.R. Holmes, R.P. Bayer, A Simple Method for the Direct Oxidation of Aromatic Amines to Nitroso Compounds1, Journal of the American Chemical Society, 82 (1960) 3454-3456, 10.1021/ja01498a054I.

[43] G. Sheldrick, SHELXT - Integrated space-group and crystal-structure determination, Acta Crystallographica Section A, 71 (2015) 3-8, doi:10.1107/S2053273314026370I.

[44] G. Sheldrick, Crystal structure refinement with SHELXL, Acta Crystallographica Section C, 71 (2015) 3-8, doi:10.1107/S2053229614024218I.

[45] P. Thordarson, Determining association constants from titration experiments in supramolecular chemistry, Chemical Society Reviews, 40 (2011) 1305-1323, 10.1039/C0CS00062KI.

[46] J.P. Patterson, M.P. Robin, C. Chassenieux, O. Colombani, R.K. O'Reilly, The analysis of solution self-assembled polymeric nanomaterials, Chemical Society Reviews, 43 (2014) 2412-2425,

[47] W.A. Velema, W. Szymanski, B.L. Feringa, Photopharmacology: Beyond Proof of Principle, Journal of the American Chemical Society, 136 (2014) 2178-2191, 10.1021/ja413063eI.

[48] I.K. Lednev, T.-Q. Ye, L.C. Abbott, R.E. Hester, J.N. Moore, Photoisomerization of a Capped Azobenzene in Solution Probed by Ultrafast Time-Resolved Electronic Absorption Spectroscopy, The Journal of Physical Chemistry A, 102 (1998) 9161-9166, 10.1021/jp982368cI.

[49] S. Iamsaard, E. Anger, S.J. Aßhoff, A. Depauw, S.P. Fletcher, N. Katsonis, Fluorinated Azobenzenes for Shape-Persistent Liquid Crystal Polymer Networks, Angewandte Chemie International Edition, 55 (2016) 9908-9912, https://doi.org/10.1002/anie.201603579I.

[50] M. Wegener, M.J. Hansen, A.J.M. Driessen, W. Szymanski, B.L. Feringa, Photocontrol of Antibacterial Activity: Shifting from UV to Red Light Activation, Journal of the American Chemical Society, 139 (2017) 17979-17986, 10.1021/jacs.7b09281I.

[51] A.A. Beharry, G.A. Woolley, Azobenzene photoswitches for biomolecules, Chemical Society Reviews, 40 (2011) 4422-4437, 10.1039/C1CS15023EI.

[52] S. Jia, W.-K. Fong, B. Graham, B.J. Boyd, Photoswitchable Molecules in Long-Wavelength Light-Responsive Drug Delivery: From Molecular Design to Applications, Chemistry of Materials, 30 (2018) 2873-2887, 10.1021/acs.chemmater.8b00357I.

[53] C. Nie, C. Liu, S. Sun, S. Wu, Visible-Light-Controlled Azobenzene-Cyclodextrin Host-Guest Interactions for Biomedical Applications and Surface Functionalization, ChemPhotoChem, 5 (2021) 893-901, https://doi.org/10.1002/cptc.202100085I.

[54] P. Weis, S. Wu, Light-Switchable Azobenzene-Containing Macromolecules: From UV to Near Infrared, Macromolecular Rapid Communications, 39 (2018) 1700220, https://doi.org/10.1002/marc.201700220I.

[55] Z. Yang, Z. Liu, L. Yuan, Recent Advances of Photoresponsive Supramolecular Switches, Asian Journal of Organic Chemistry, 10 (2021) 74-90, https://doi.org/10.1002/ajoc.202000501I.

[56] H. Yan, Y. Qiu, J. Wang, Q. Jiang, H. Wang, Y. Liao, X. Xie, Wholly Visible-Light-Responsive Host–Guest Supramolecular Gels Based on Methoxy Azobenzene and β-Cyclodextrin Dimers, Langmuir, 36 (2020) 7408-7417, 10.1021/acs.langmuir.0c00964I.

[57] L. Zhang, H. Zhang, F. Gao, H. Peng, Y. Ruan, Y. Xu, W. Weng, Host-guest interaction between fluoro-substituted azobenzene derivative and cyclodextrins, RSC Advances, 5 (2015) 12007-12014, 10.1039/C4RA13283AI.

[58] D. Wang, M. Wagner, H.-J. Butt, S. Wu, Supramolecular hydrogels constructed by red-light-responsive host-guest interactions for photo-controlled protein release in deep tissue, Soft Matter, 11 (2015) 7656-7662, 10.1039/C5SM01888AI.

[59] D. Brynn Hibbert, P. Thordarson, The death of the Job plot, transparency, open science and online tools, uncertainty estimation methods and other developments in supramolecular chemistry data analysis, Chemical Communications, 52 (2016) 12792-12805, 10.1039/C6CC03888CI.

[60] C. Gourier, E. Beaudoin, M. Duval, D. Sarazin, S. Maître, J. François, A Light Scattering Study of the Association of Hydrophobically α- and α,ω-End-capped Poly(ethylene oxide) in Water, Journal of Colloid and Interface Science, 230 (2000) 41-52, https://doi.org/10.1006/jcis.2000.7033I.

[61] R.F. Tabor, T.M. McCoy, Y. Hu, B.L. Wilkinson, Physicochemical and Biological Characterisation of Azobenzene-Containing Photoswitchable Surfactants, Bulletin of the Chemical Society of Japan, 91 (2018) 932-939, 10.1246/bcsj.20180024I.

[62] F. Renou, T. Nicolai, E. Nicol, L. Benyahia, Structure and Viscoelasticity of Mixed Micelles Formed by Poly(ethylene oxide) End Capped with Alkyl Groups of Different Length, Langmuir, 25 (2009) 515-521, 10.1021/la802708mI.

[63] C. Boutris, E.G. Chatzi, C. Kiparissides, Characterization of the LCST behaviour of aqueous poly(N-isopropylacrylamide) solutions by thermal and cloud point techniques, Polymer, 38 (1997) 2567-2570, https://doi.org/10.1016/S0032-3861(97)01024-0I.

[64] D. Kungwatchakun, M. Irie, Photoresponsive polymers. Photocontrol of the phase separation temperature of aqueous solutions of poly-[N-isopropylacrylamide-co-N-(4-phenylazophenyl)acrylamide], Die Makromolekulare Chemie, Rapid Communications, 9 (1988) 243-246, https://doi.org/10.1002/marc.1988.030090408I.

[65] A. Desponds, R. Freitag, Synthesis and Characterization of Photoresponsive N-Isopropylacrylamide Cotelomers, Langmuir, 19 (2003) 6261-6270, 10.1021/la020944xI.

[66] F.D. Jochum, L. zur Borg, P.J. Roth, P. Theato, Thermo- and Light-Responsive Polymers Containing Photoswitchable Azobenzene End Groups, Macromolecules, 42 (2009) 7854-7862, 10.1021/ma901295fI.

[67] Y.-J. Liu, A. Pallier, J. Sun, S. Rudiuk, D. Baigl, M. Piel, E. Marie, C. Tribet, Non-monotonous variation of the LCST of light-responsive, amphiphilic poly(NIPAM) derivatives, Soft Matter, 8 (2012) 8446-8455, 10.1039/C2SM25959AI.

[68] P. Ravi, S.L. Sin, L.H. Gan, Y.Y. Gan, K.C. Tam, X.L. Xia, X. Hu, New water soluble azobenzene-containing diblock copolymers: synthesis and aggregation behavior, Polymer, 46 (2005) 137-146, https://doi.org/10.1016/j.polymer.2004.11.009I.

[69] L. Zhang, J. Li, H. Liu, Thermal inverse phase transition of azobenzene hydroxypropylcellulose in aqueous solutions, Cellulose, 23 (2016), 10.1007/s10570-016-0878-1I.

[70] T. Ueki, A. Yamaguchi, N. Ito, K. Kodama, J. Sakamoto, K. Ueno, H. Kokubo, M. Watanabe, Photoisomerization-Induced Tunable LCST Phase Separation of Azobenzene-Containing Polymers in an Ionic Liquid, Langmuir, 25 (2009) 8845-8848, 10.1021/la901159rI.

[71] X. Ma, X. Lan, L. Wu, L. Wang, Q. Gu, Y. Shi, X. Gu, Z. Luo, Photo-induced actuator using temperature and light dual responsive azobenzene containing ion gel in ionic liquid, European Polymer Journal, 123 (2020) 109446, https://doi.org/10.1016/j.eurpolymj.2019.109446I.

[72] F. Zhao, A. Bonasera, U. Nöchel, M. Behl, D. Bléger, Reversible Modulation of Elasticity in Fluoroazobenzene-Containing Hydrogels Using Green and Blue Light, Macromolecular Rapid Communications, 39 (2018) 1700527, https://doi.org/10.1002/marc.201700527I.

[73] Y.B. Mok, M.W. Noh, G.C. Kim, Y.J. Song, H. Kim, S. Kim, S. Yi, J.H. Seo, Y. Lee, Light-tunable thermoresponsive behavior of branched polyethylenimine derivatives in water, Polymer, 107 (2016) 37-43, https://doi.org/10.1016/j.polymer.2016.11.014I.

[74] R. Dong, B. Zhu, Y. Zhou, D. Yan, X. Zhu, Reversible photoisomerization of azobenzene-containing polymeric systems driven by visible light, Polymer Chemistry, 4 (2013) 912-915, 10.1039/C2PY21060FI.

[75] J.-H. Kim, E. Koo, S.-Y. Ju, W.-D. Jang, Multimodal Stimuli-Responsive Poly(2-isopropyl-2-oxazoline) with Dual Molecular Logic Gate Operations, Macromolecules, 48 (2015) 4951-4956, 10.1021/acs.macromol.5b01046I.

[76] A. Housni, Y. Zhao, Y. Zhao, Using Polymers To Photoswitch the Aggregation State of Gold Nanoparticles in Aqueous Solution, Langmuir, 26 (2010) 12366-12370, 10.1021/la101798xI.

[77] A. Bergen, S. Rudiuk, M. Morel, T. Le Saux, H. Ihmels, D. Baigl, Photodependent Melting of Unmodified DNA Using a Photosensitive Intercalator: A New and Generic Tool for Photoreversible Assembly of DNA Nanostructures at Constant Temperature, Nano Letters, 16 (2016) 773-780, 10.1021/acs.nanolett.5b04762I.

[78] L. Zhang, L. Zhao, Y. Ling, H. Tang, Unusual light-tunable thermoresponsive behavior of OEGylated homopolypeptide with azobenzene and thioether spacers, European Polymer Journal, 111 (2019) 38-42, https://doi.org/10.1016/j.eurpolymj.2018.12.013I.

Supporting information

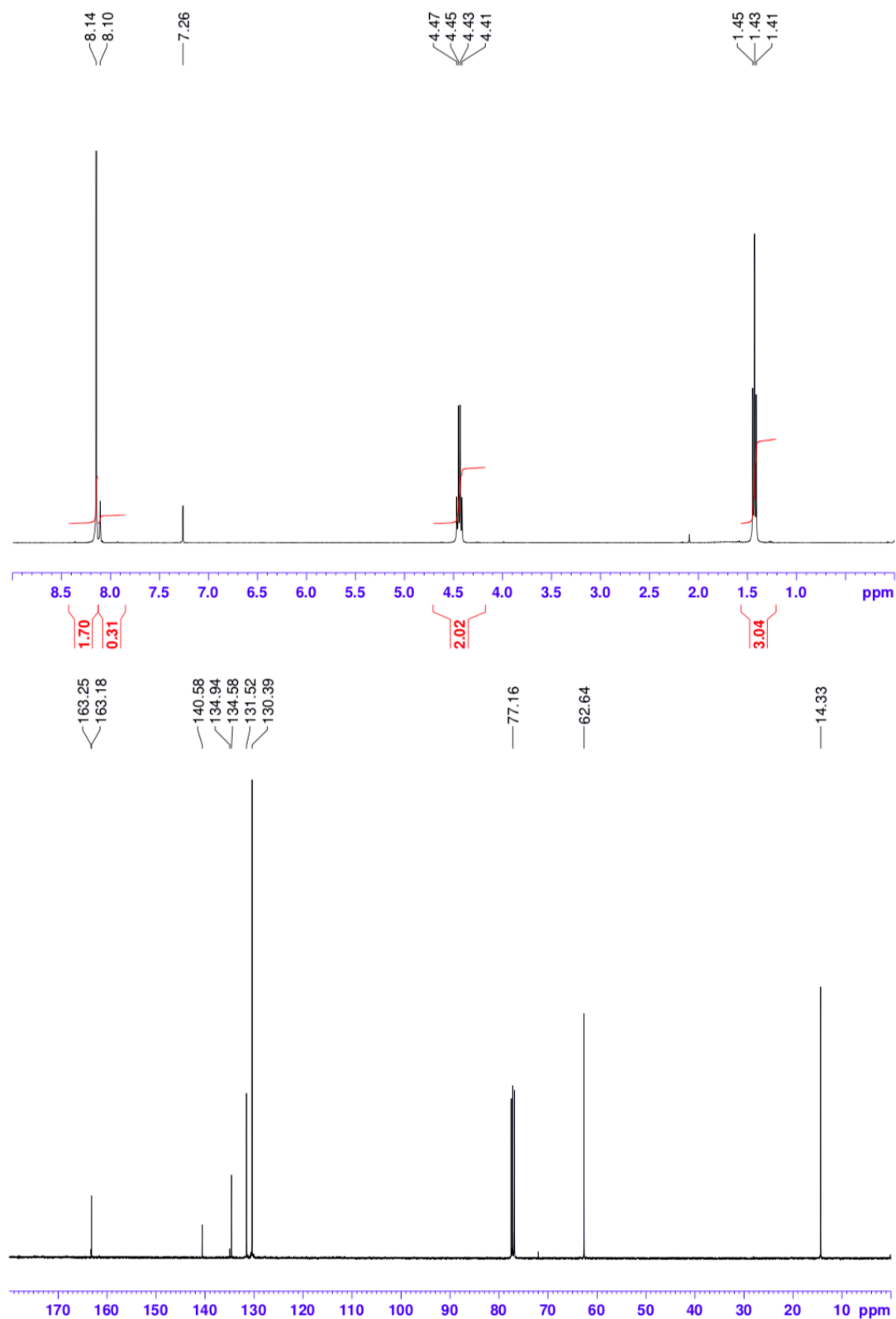## 1. Characterization of 2Cl2F-AZO-PEO

Figure S1. ^{1}H NMR spectra (400 MHz, CDCl$_3$) and ^{13}C NMR spectrum (100 MHz, CDCl$_3$) of intermediate **2**.
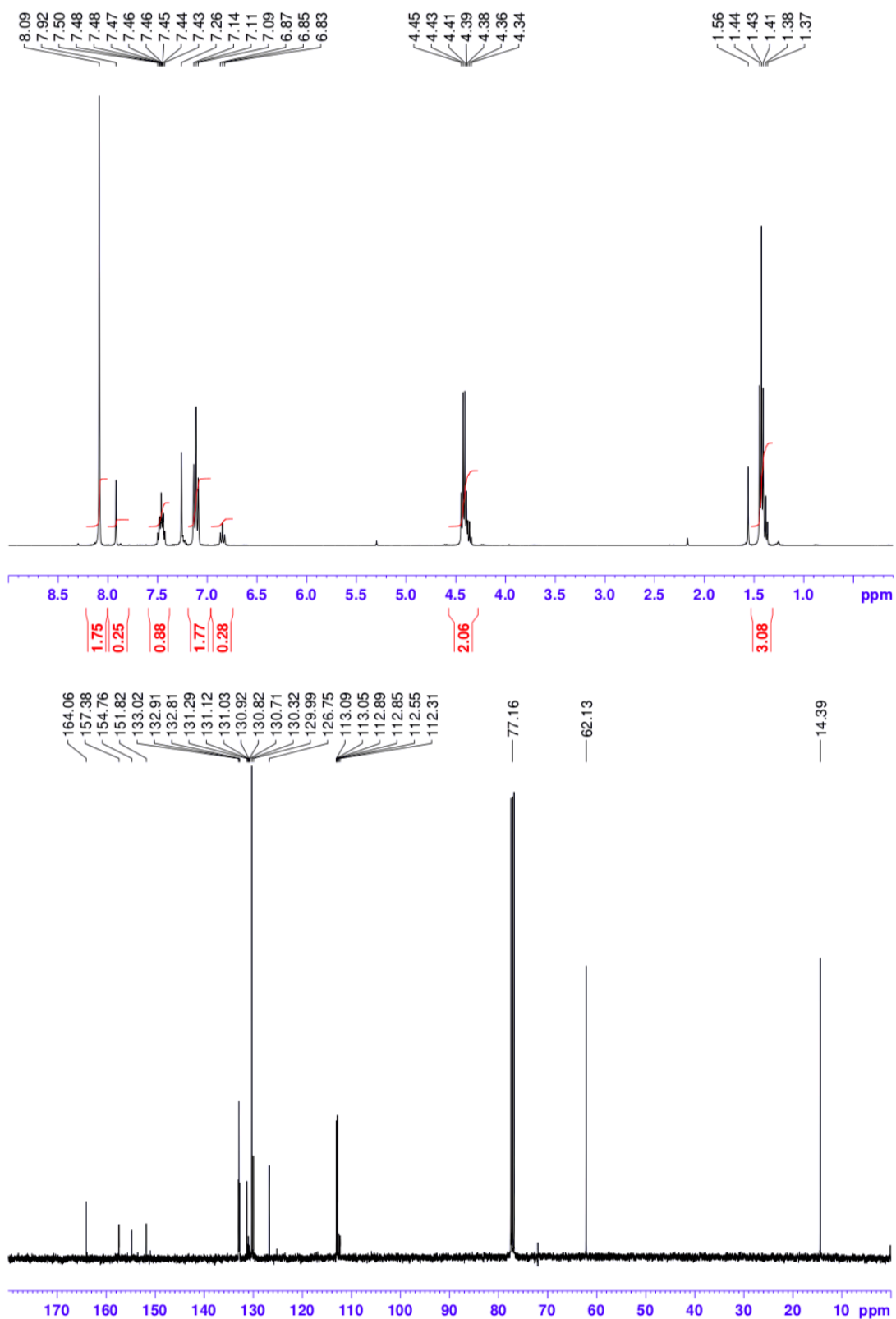
Figure S2. ^{1}H NMR spectrum (400 MHz, CDCl$_3$) and ^{13}C NMR spectrum (100 MHz, CDCl$_3$) of intermediate **3**, containing primarily the *trans* isomer, and a small amount (~ 13 %) of the *cis* isomer.
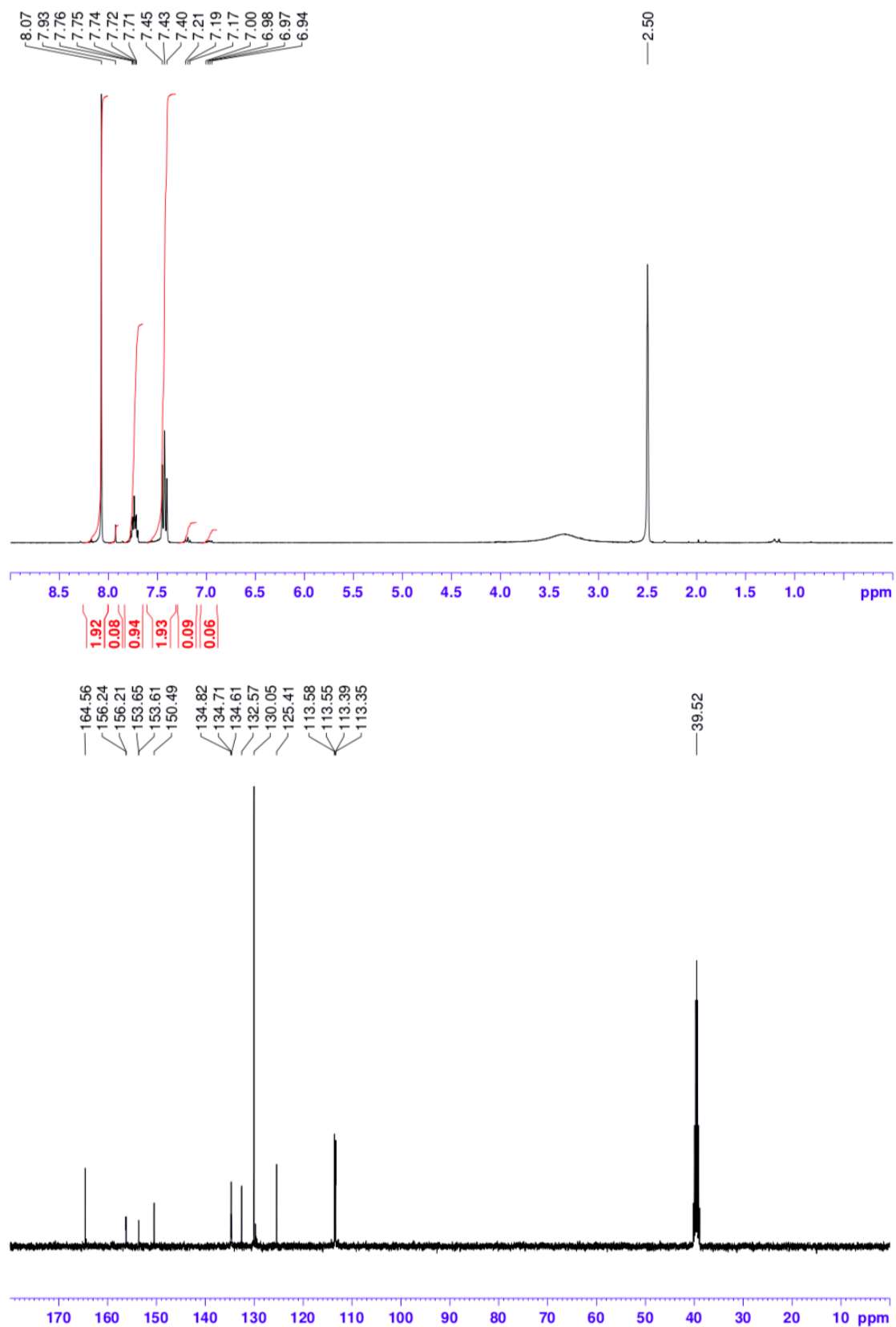
Figure S3. ^{1}H NMR spectrum (400 MHz, d_6-DMSO) and ^{13}C NMR spectrum (100 MHz, d_6-DMSO) of intermediate **4**, containing almost exclusively the *trans* isomer.
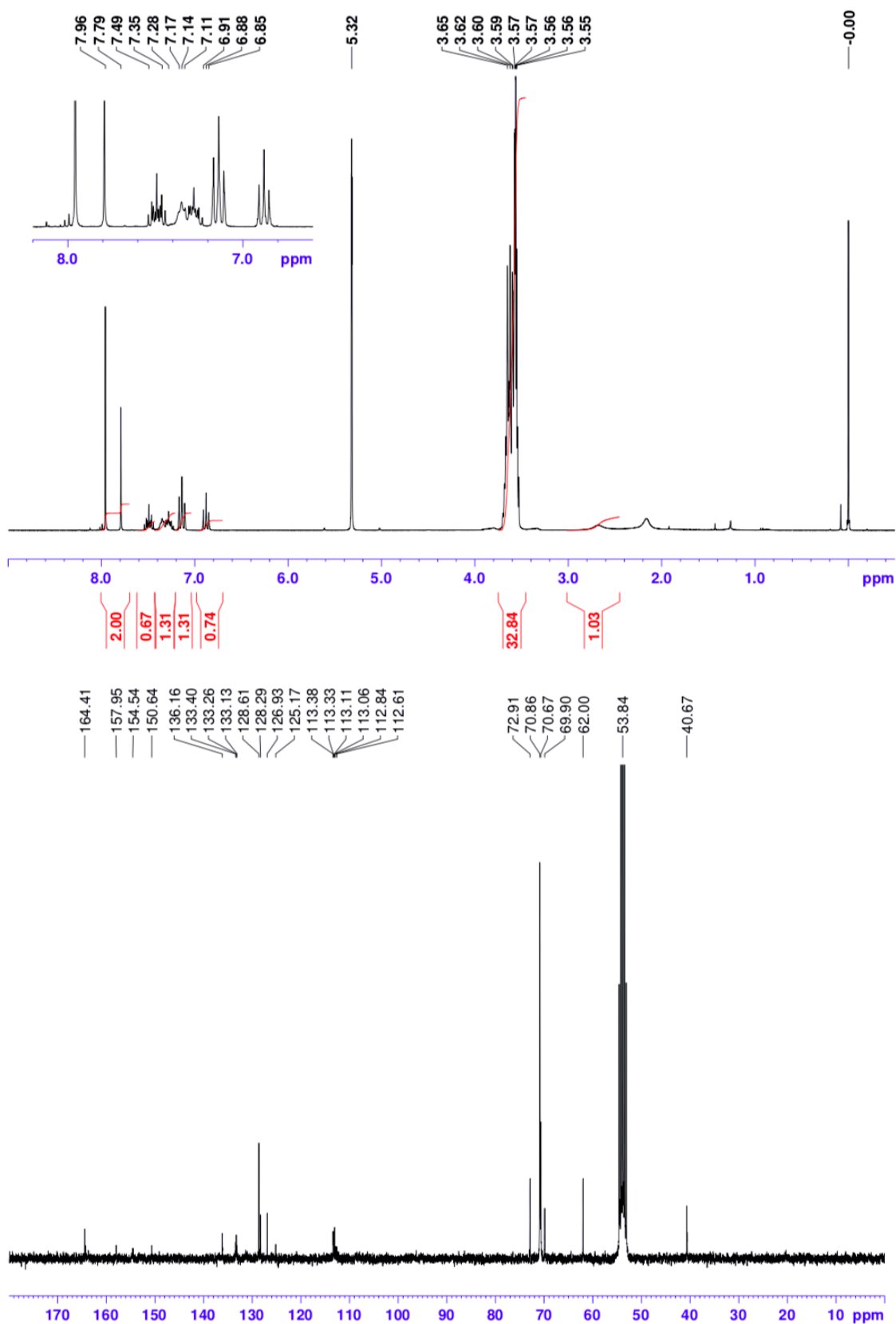
Figure S4. ^{1}H NMR spectrum (400 MHz, d$_6$-DMSO) and ^{13}C NMR spectrum (100 MHz, d$_6$-DMSO) of 2Cl2F-AZO-PEO, containing a mixture of *trans* and *cis* isomers.
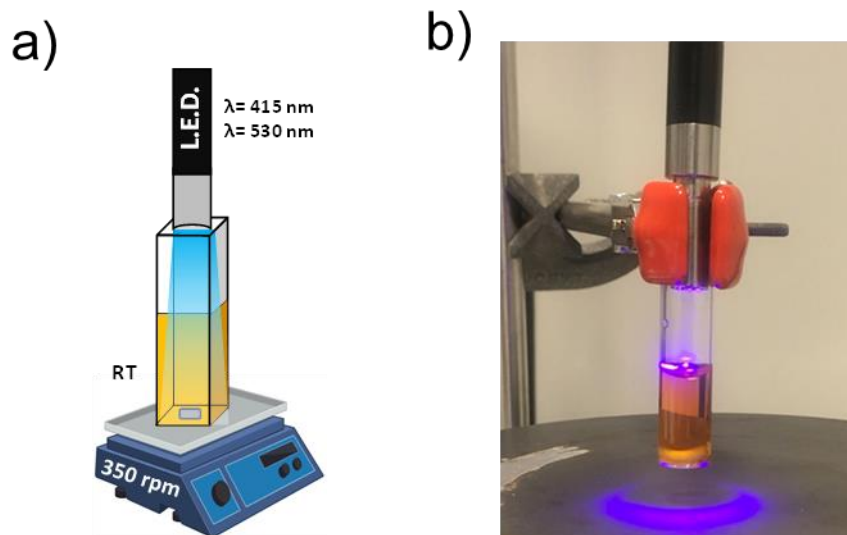
Figure S5. a) Scheme and b) photography of the experimental setup employed during the sample irradiation.

Table S1. Kinetic data and thermodynamic parameters as calculated using the Arrhenius and Eyring equations for thermal *trans* to *cis* isomerization in CD_3CN of compound **3**, with estimate of kinetic values at body temperature (37 °C).

	k (s^{-1}) 37 °C	$\tau_{1/2}$ (h) 37 °C	A (s^{-1})	E_a (kJ•mol^{-1})	$\Delta H^{\ddagger}$ (kJ•mol^{-1})	$\Delta S^{\ddagger}$ (J•mol^{-1})	$\Delta G^{\ddagger}$ (kJ•mol^{-1})
3	$1.0 \cdot 10^{-5}$	19	$2.9 \cdot 10^{12}$	104	101	-15	106

2. Thermal stability
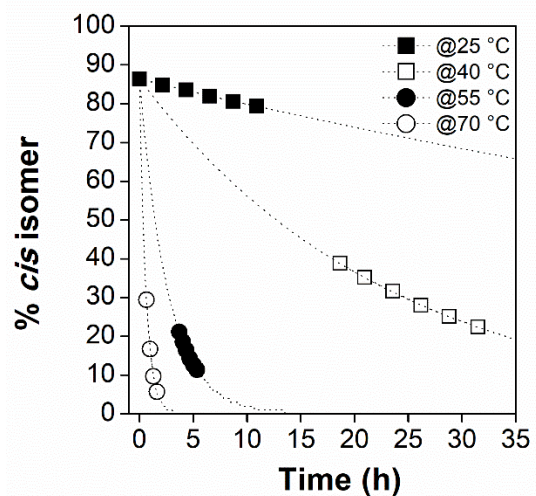
Figure S6. ^{1}H NMR studies (CD$_3$CN, 400 MHz) of the thermal relaxation of *cis*-**3** in the dark at various temperatures. The dotted lines represent fits by equation (1). Note that for easier visual comparison, the first data point for all curves was shifted so that the fitted lines all commence at the 25 °C starting point. This has no influence on the derived kinetic parameters.
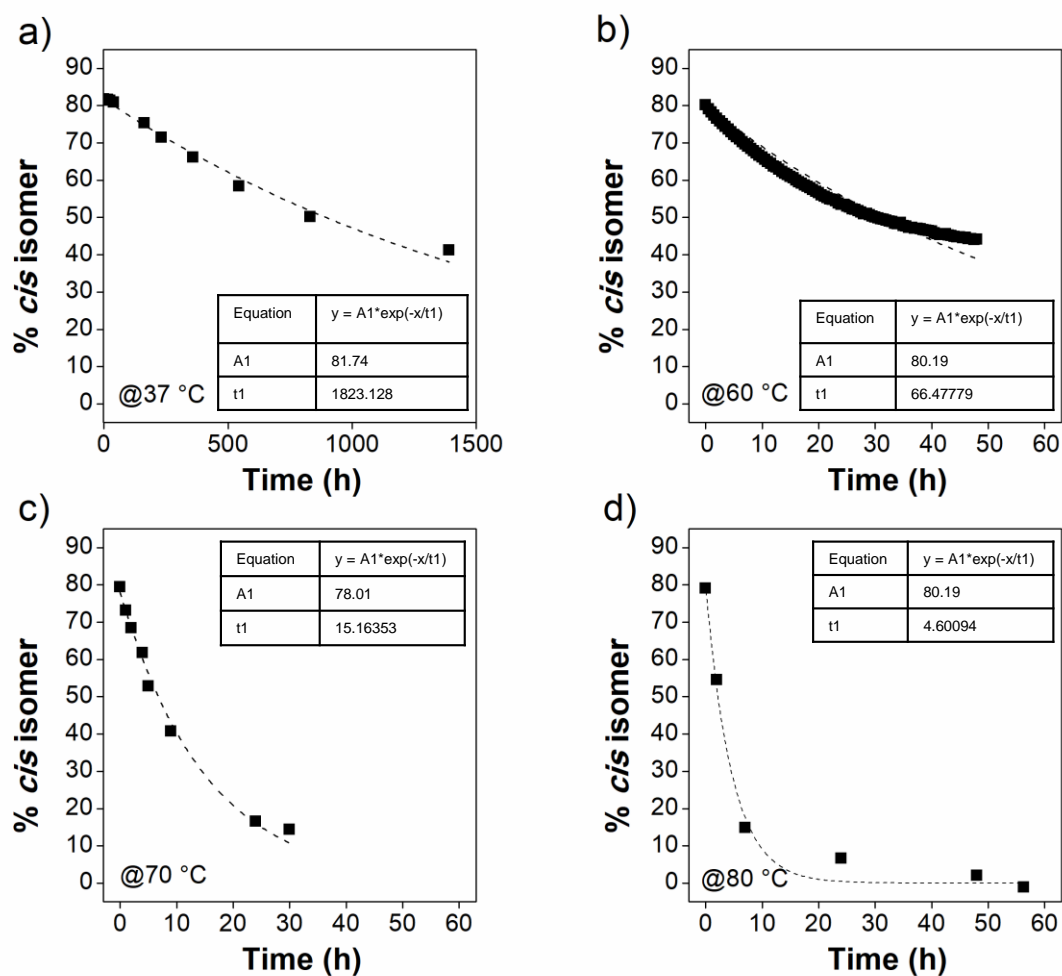
Figure S7. Thermal 4F-AZO-PEO *cis* to *trans* isomerization in water: plots of % *cis* isomer (as determined by UV-vis spectroscopy) following the time at a) 37 °C, b) 60 °C, c) 70 °C and d) 80 °C. The decrease in *cis* isomer was fitted by a first order exponential decay 1 using Origin software.
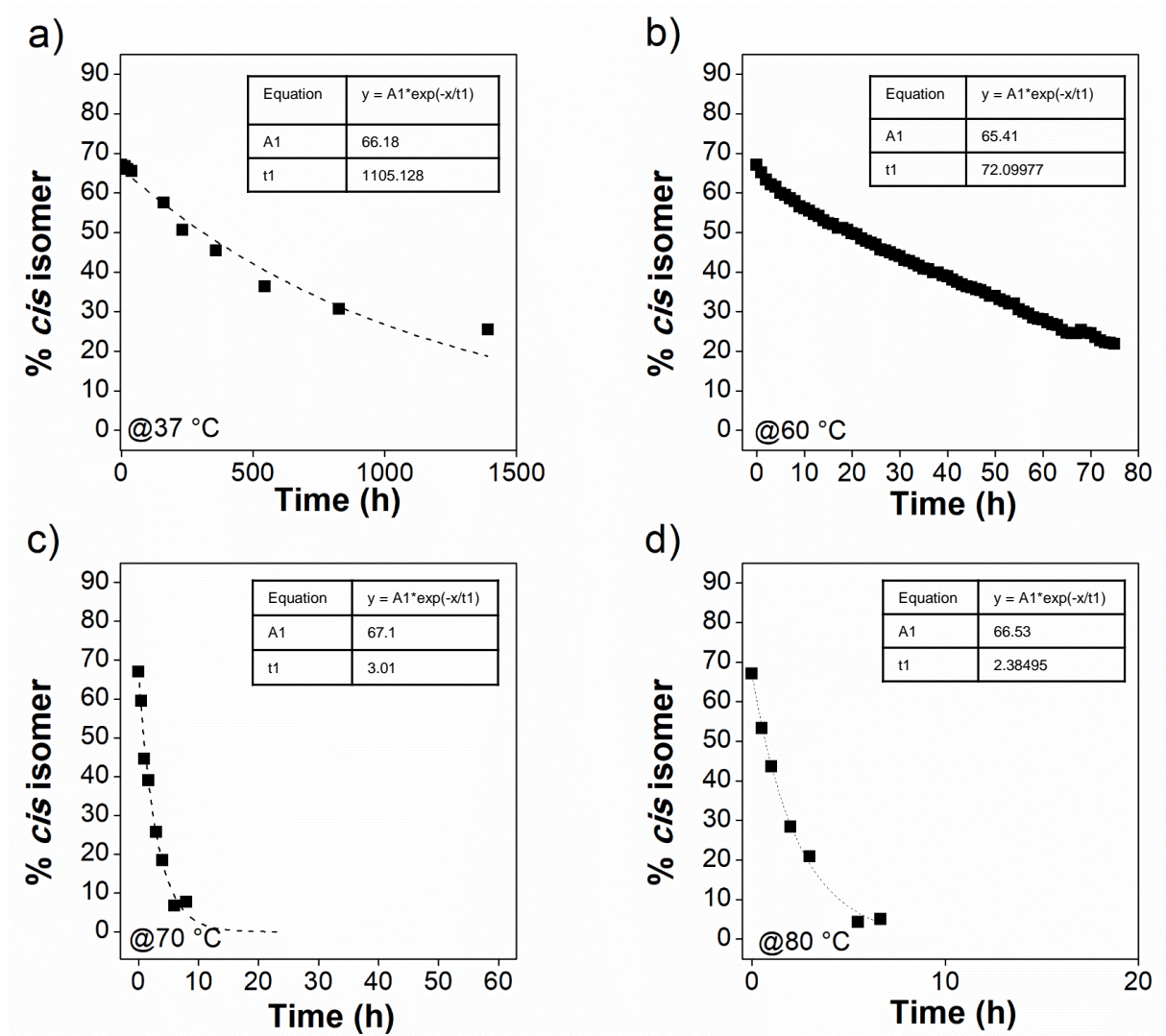
Figure S8. Thermal 2Cl2F-AZO-PEO *cis* to *trans* isomerization in water: plots of % *cis* isomer (as determined by UV-vis spectroscopy) following the time at a) 37 °C, b) 60 °C, c) 70 °C and d) 80 °C. The decrease in *cis* isomer was fitted by a first order exponential decay 1 using Origin software.
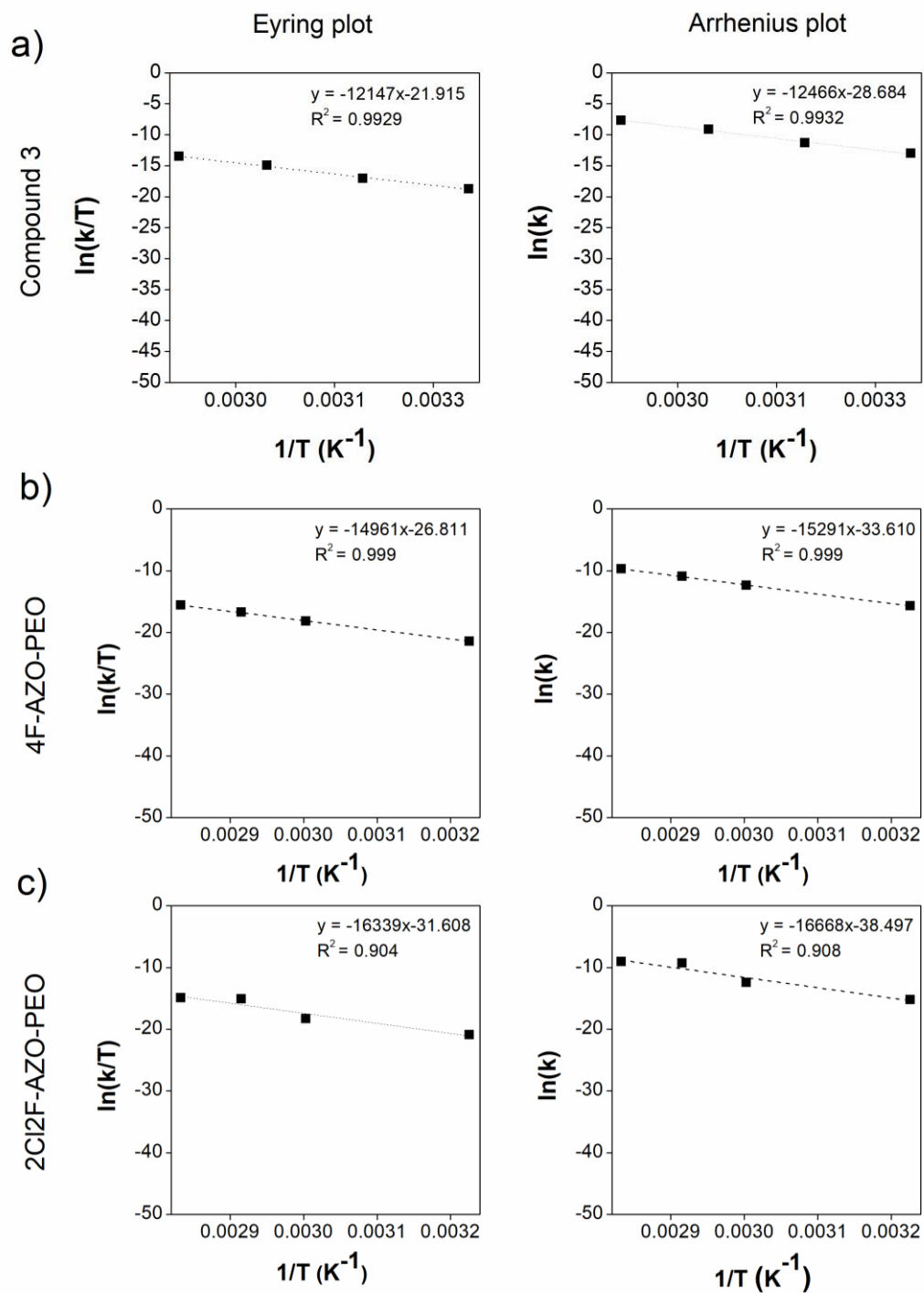
Figure S9. Derived Eyring and Arrhenius plots from the a) ^{1}H NMR spectra (CD$_3$CN, 400 MHz) of the thermal relaxation of **3** and the UV-Visible spectroscopy measurement (H$_2$O) of the thermal relaxation of b) 4F-AZO-PEO and c) 2Cl2F-AZO-PEO in the dark following the temperature.

3. Complexation with β-CD
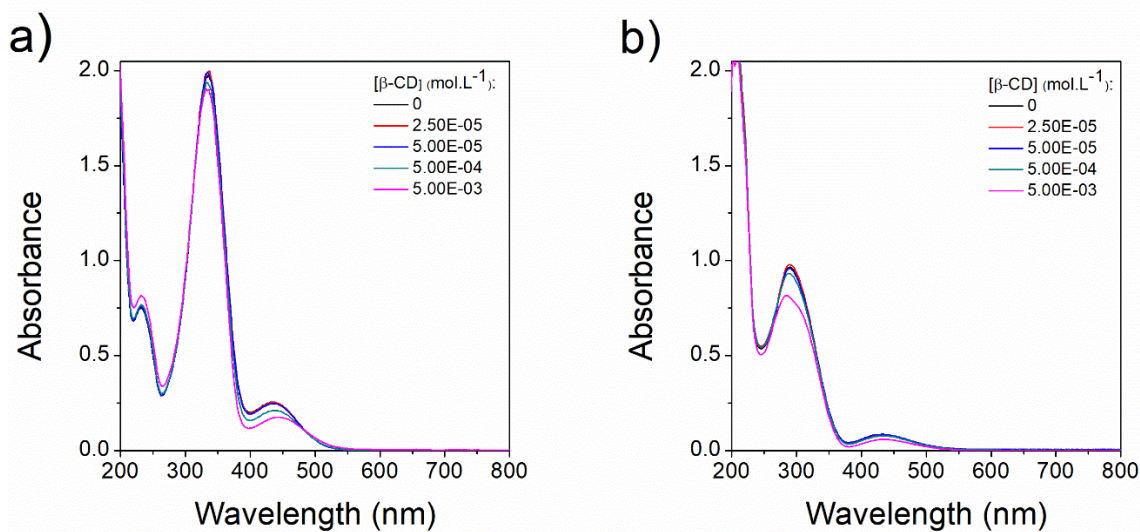
Figure S10: UV-Visible spectra of a) *trans*-rich (91% *trans*) 4F-AZO-PEO and b) *trans*-rich (83% *trans*) 2Cl2F-AZO-PEO with different content of β-CD.
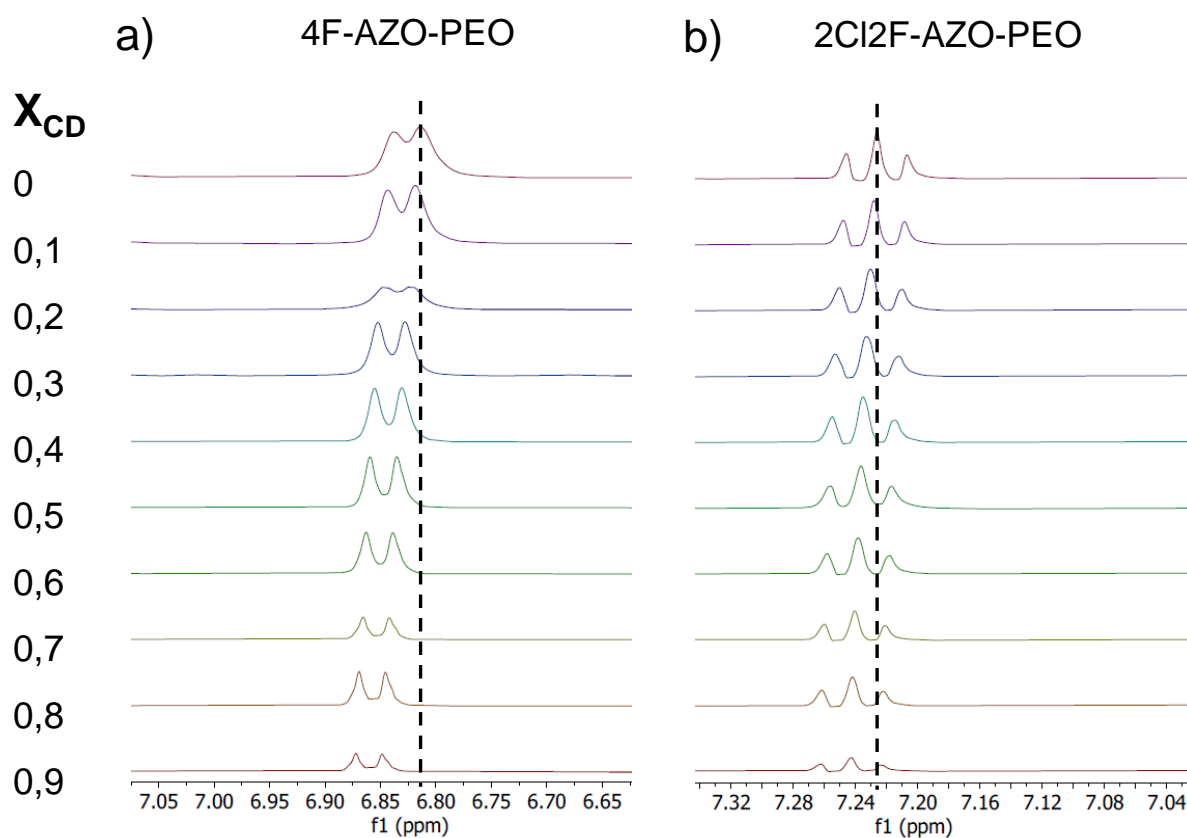
Figure S11. ^{1}H NMR spectra focusing on characteristic peaks of the a) *trans*-rich (91% *trans*) 4F-AZO-PEO and b) *trans*-rich (83% *trans*) 2Cl2F-AZO-PEO involved in the complexation with the β-CD.
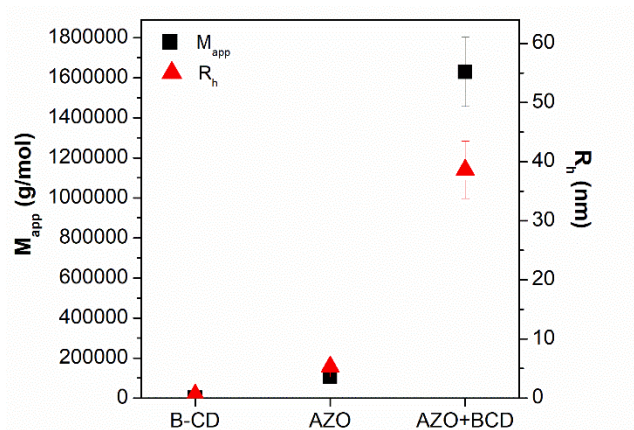
Figure S12. Evidence of PSS(415)*trans* 4F-AZO-PEO@β-CD inclusion complex formation by light scattering experiments. Results are presented as mean ± standard deviation from the measured angles. The apparent molar mass (M_{app}) of the complexed aggregates increased 16 and 1 500 times (1 600 000 g•mol^{-1}) compared to those of the 4F-AZO-PEO aggregates (100 000 g•mol^{-1}, *vide infra*) or to the β-CD alone (1 100 g.mol^{-1}).
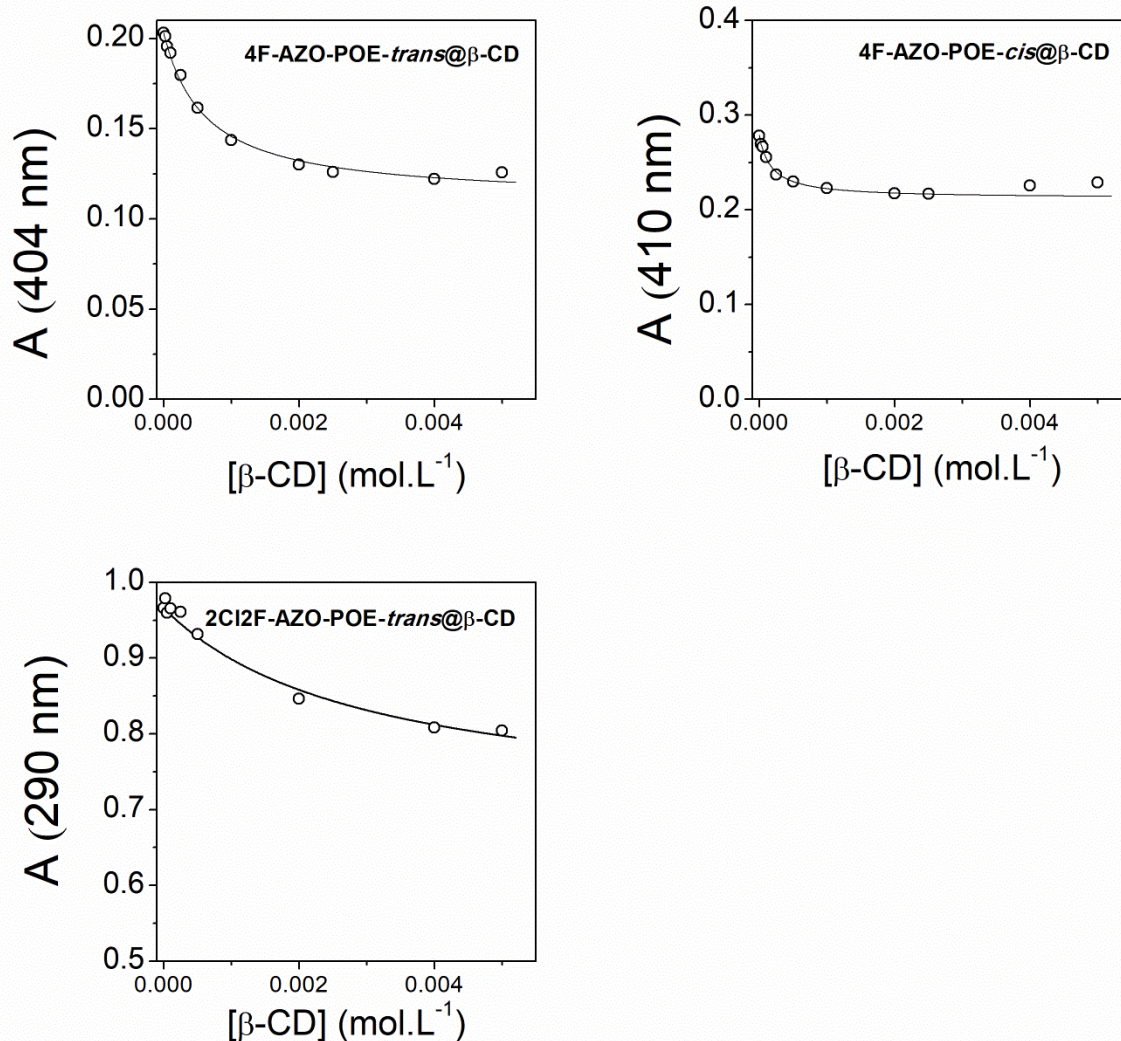
Figure S13. Evolution of the absorbance of the 4F-AZO-PEO-*trans*@β-CD, 4F-AZO-PEO-*cis*@β-CD and 2Cl2F-AZO-PEO-*trans*@β-CD complexes studied at 404 nm, 410 nm and 290 nm respectively with the addition of β-CD. The modeling is represented in full line. AZO-PEO-*trans* stands for the *trans*-rich mixture for each azobenzene derivative while 4F-AZO-PEO-*cis* is the PSS(365)*cis* of 4F-AZO-PEO.

Modeling:

A homemade software called SA (Simulation – Adjustment, available for downloading at http://cinet.chim.pagesperso-orange.fr/tele_sa/install_Sa_Eng.html) was used to fit the experimental data of titration experiments.

Association constants determination:

Model for a 1:1 complexation between azobenzene derivative (AZO) and β-CD :

$$AZO + β\text{-}CD \underset{k_{-1}}{\overset{k_1}{\rightleftharpoons}} AZO@β\text{-}CD \qquad Ka = \frac{[AZO@β-CD]}{[AZO][β-CD]} = \frac{k_1}{k_{-1}} \quad (1)$$
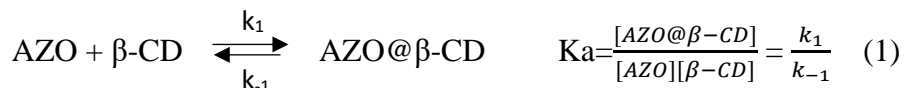
Where AZO@β-CD represent the complex. UV-Visible absorption at the studied wavelength is related to the concentrations of free AZO and AZO@β-CD complex according to equation (2).

$$A = A_{AZO} + A_{AZO@β\text{-}CD} \ (2)$$

In the calculation procedure, for *cis* and *trans* 4F-AZO-PEO and *trans* 2Cl2F-AZO-PEO, the parameters to extract are the rate constant ratio (k_1/k_{-1}) and the extinction coefficient of the inclusion complex. For that, constant k_{-1} is fixed to an arbitrary value and only k_1 is adjusted. This implies that the spectrum of the free AZO is known which is the case for the three up-mentioned compound assuming that we consider pure isomers as starting compounds. In the case of *cis* 2Cl2F-AZO-PEO such approximation is no longer valid and the overlap of the absorption spectra indeterminacy on the desired parameters.
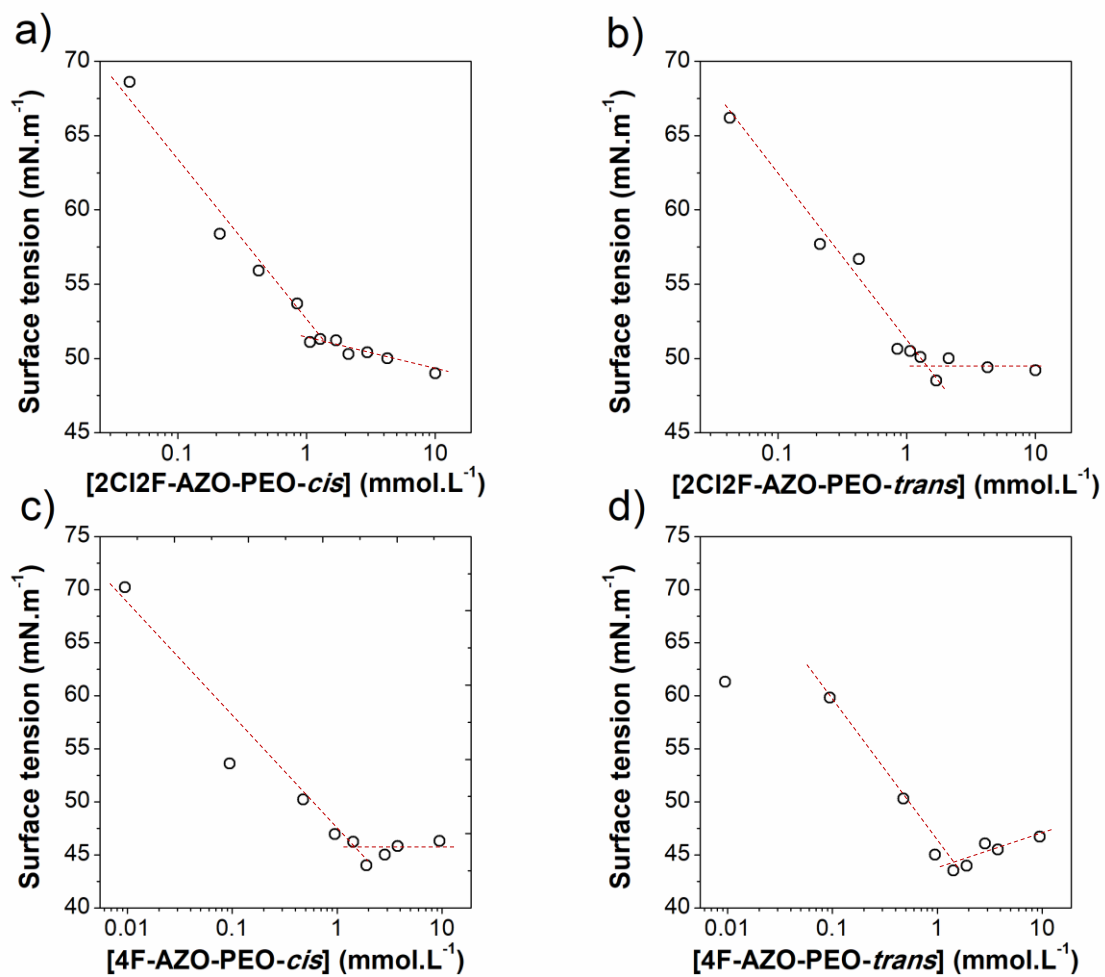
4. Surface tension

Figure S14. Critical micellar concentration of a) *cis*-2Cl2F-AZO-PEO, b) *trans*-2Cl2F-AZO-PEO at 23 °C, c) *cis*-4F-AZO-PEO and d) *trans*-4F-AZO-PEO at 4 °C.
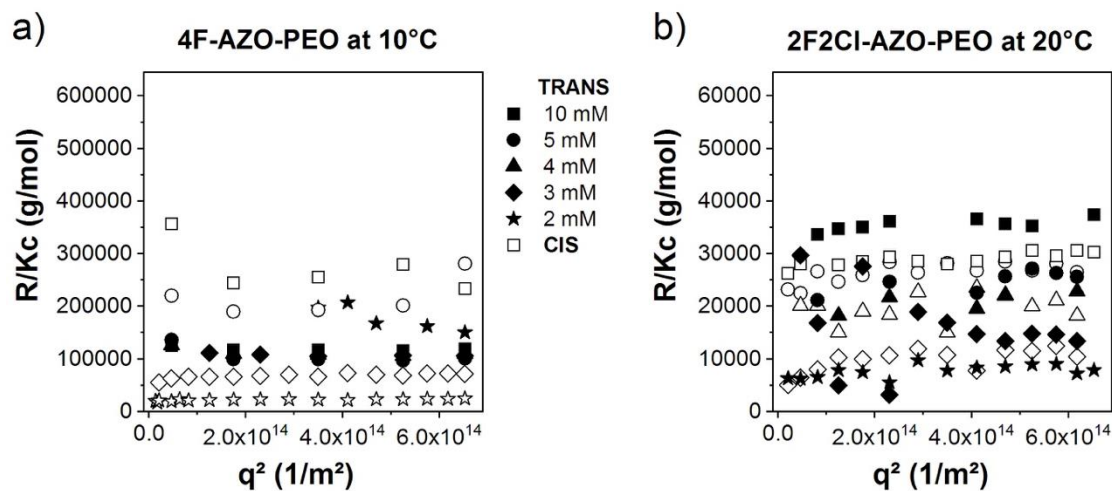
5. Light scattering

Figure S15. Dependence of the R/Kc as a function of the scattering vector (q^2) for a) 4F-AZO-PEO at 10 °C and b) 2Cl2F-AZO-PEO at 20°C in *trans* and *cis* configuration at different concentrations.
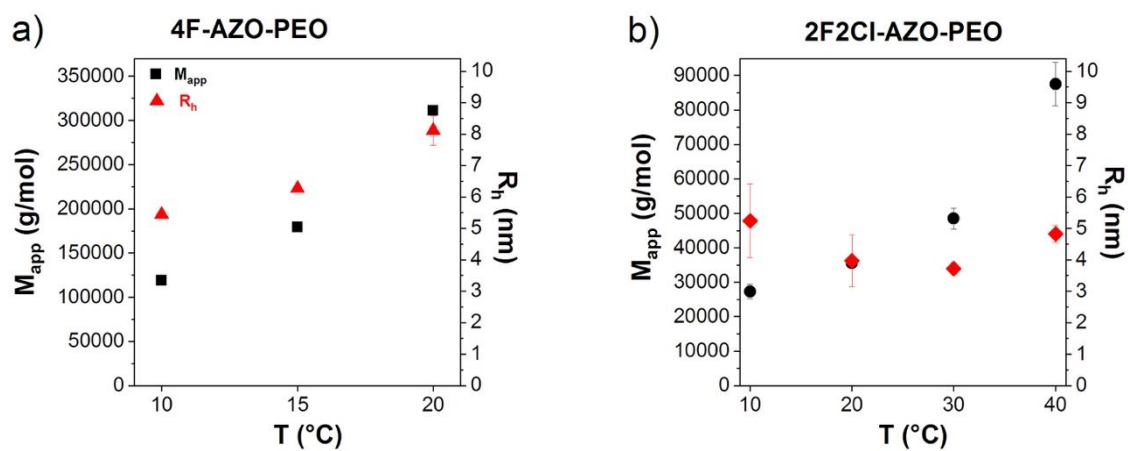

Figure S16. Temperature dependence of the apparent molar mass (M_{app}) (black symbols) and hydrodynamic radius (R_h) (red symbols) of a) *trans*-4F-AZO-PEO and b) *trans*-2Cl2F-AZO-PEO at 10 mM.

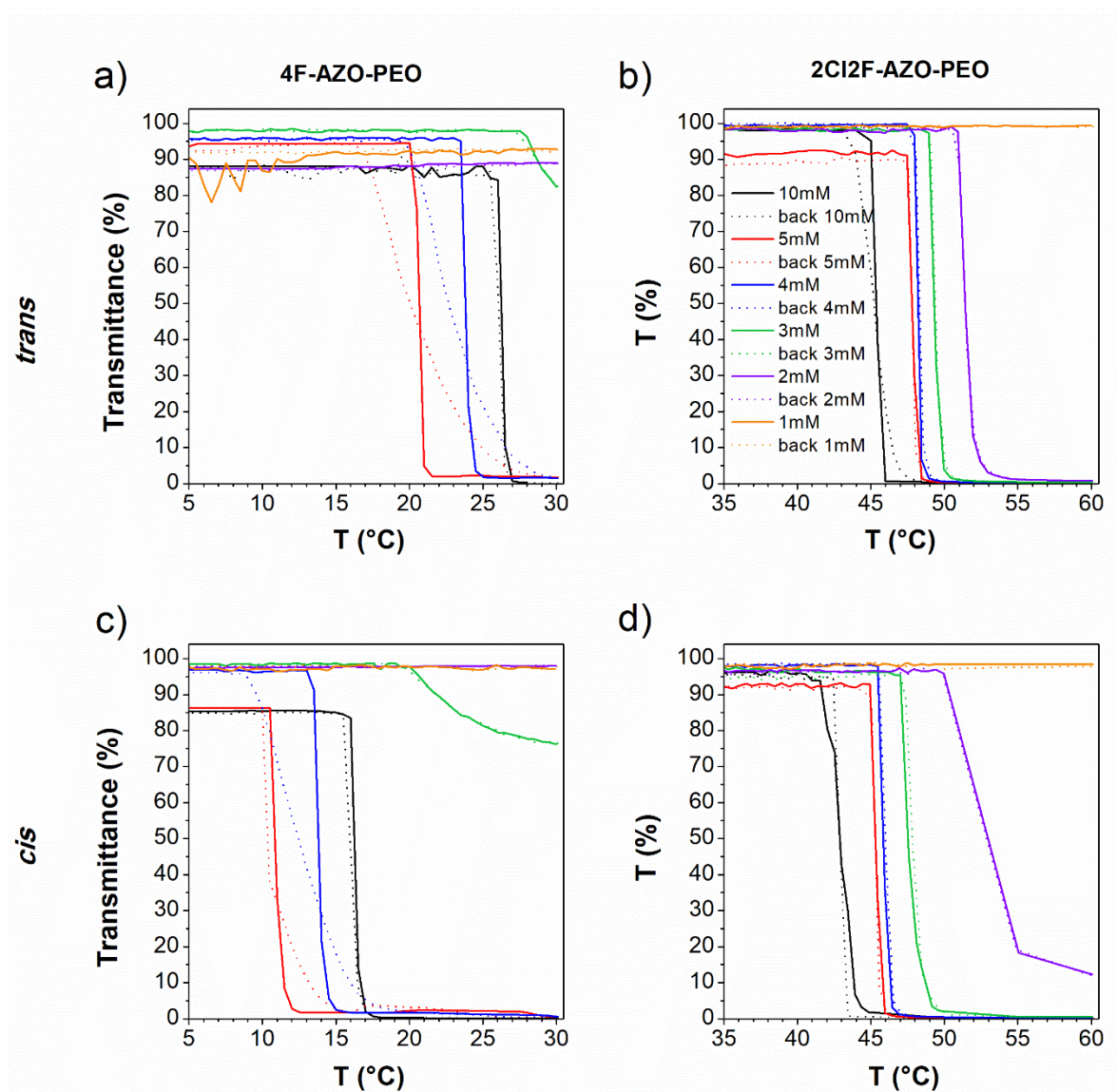## 6. UV-Vis spectroscopy - LCST

Figure S17. Evolution of the transmittance following the temperature for a) *trans*-4F-AZO-PEO b) *trans*-2Cl2F-AZO-PEO c) *cis*-4F-AZO-PEO and d) *cis*-2Cl2F-AZO-PEO at λ=700 nm at a rate of 0.5°C.min^{-1}.